Preprint of: Honarmandrad, Z., Mousavi Khadem, S. S., Kucharska, K., Kaykhaii, M., Łuczak, J., & Gębicki, J. (2025). Enhanced sorption of inhibitory compounds from fermentation broth using a MOF@pseudo-DES composite. JOURNAL OF MOLECULAR LIQUIDS, 421, 126845. https://doi.org/10.1016/j.molliq.2025.126845

Graphical Abstract

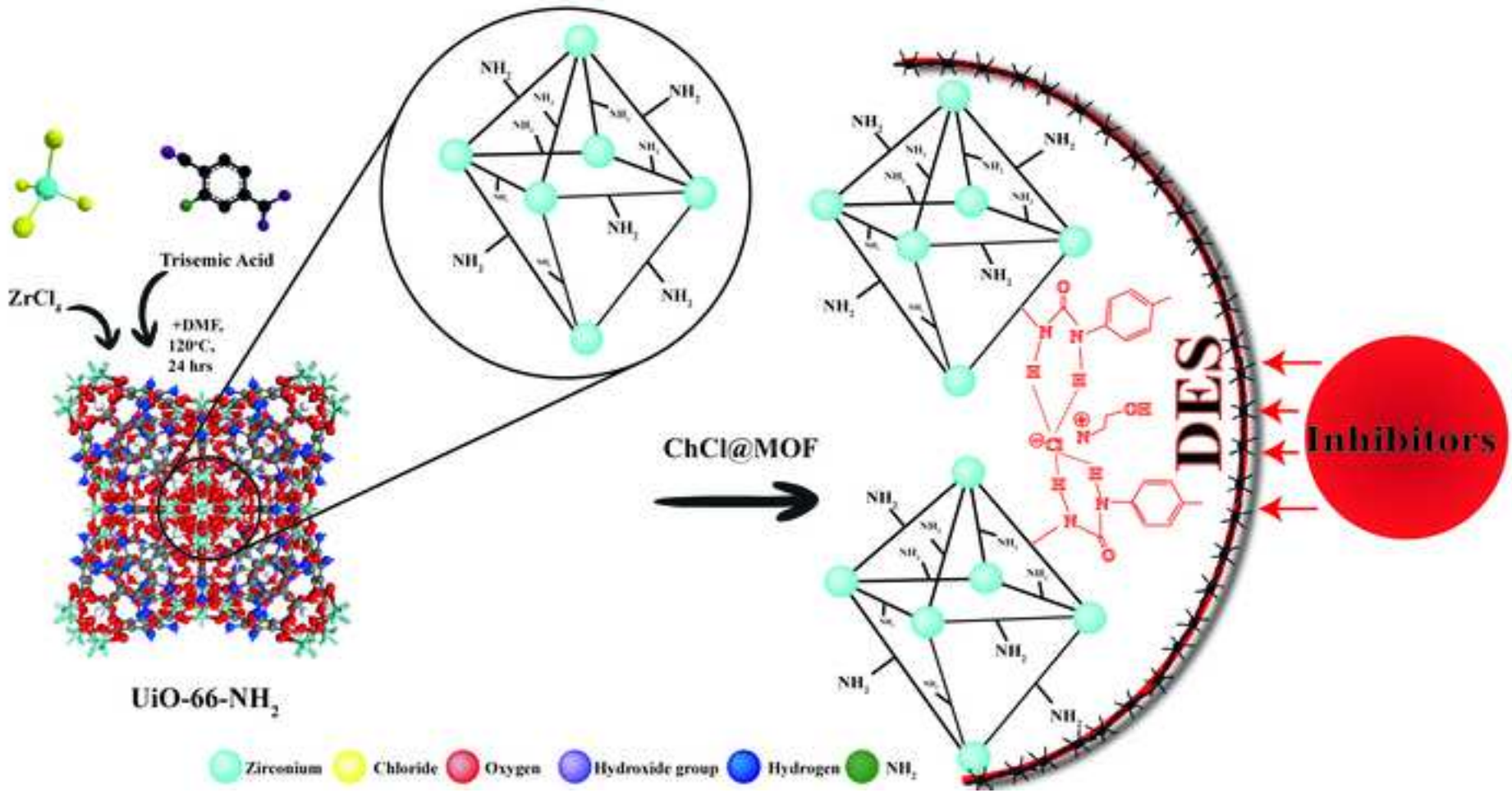

Enhanced sorption of inhibitory compounds from fermentation broth using a novel metal organic framework modified with deep eutectic solvents

Zhila Honarmandrad[a*], Seyed Soroush Mousavi Khadem[a], Karolina Kucharska[a], Massoud Kaykhaii[b], Justyna Łuczak[a], Jacek Gebicki[a]

[a]*Department of Process Engineering and Chemical Technology, Faculty of Chemistry, Gdańsk University of Technology, Narutowicza 11/12, Gdańsk 80-233, Poland*

[b]*Comenius University in Bratislava, Faculty of Natural Science, Department of Analytical Chemistry, Mlynská dolina, 842 15, Bratislava, Slovakia*

*Corresponding author. E-mail: Zhila.honarmandrad@gmail.com

ABSTRACT

The increasing interest in biorefinery and bioconversion processes underscores the need for efficient methods to enhance biohydrogen and biofuel production. However, the presence of inhibitory compounds, such as hydroquinone (HQ), 5-hydroxymethylfurfural (HMF), furfural (FF), and vanillin (VAN), in fermentation broth poses a significant challenge to these processes. These inhibitors are by-products of biomass degradation which hinder microbial growth and compromise the overall efficiency of ecosystem. This study introduces a novel and innovative approach aimed at removing these inhibitory compounds from the broths after hydrolytic pre-treatment and dark fermentation. A ChCl@NH_2-UiO-66, metal organic framework (MOF) composite was synthesized, fully characterized, and employed for the efficient sorption and removal of inhibitors present in the fermentation broth and biomass hydrolysates. To determine the effect of choline chloride on NH_2-UiO-66, the samples were characterized using X-ray

diffraction, thermogravimetry, differential thermogravimetry, Fourier transform infrared spectroscopy, BET surface area measurements, scanning electron microscopy, and energy-dispersive spectroscopy. Various parameters influencing the removal efficiency, including pH, adsorbent amount, initial inhibitor concentration, and vortex time, were systematically investigated and optimized. Under the optimal conditions, the removal efficiency of HQ, HMF, FF, and VAN was 62.08%, 56.09%, 45.29%, and 83.46% respectively, for a synthetic sample. These values for real samples after hydrolysis and prior to fermentation were exceeded 51.73%, 53.21%, 42.69%, and 37.59%, for HQ, HMF, FF, and VAN, respectively. Hydrogen bonding, electrostatic interactions, van der Waals forces, and π-π stacking between the functional groups of ChCl@NH_2-UiO-66 and the inhibitors can act as the mechanism for inhibitor removal. This groundbreaking research is the first of its kind to employ a MOF in conjunction with a deep eutectic solvent (DES) for this purpose; the results are simple, very effective, environmentally friendly, quick to react, and highly selective, making it ideal for biomass hydrolysis purification.

Keywords: Metal organic framework, Deep eutectic solvents, Biohydrogen, Phenolic derivatives, Dark fermentation

1. Introduction:

In the realm of conversion of biomass into valuable biofuels and biochemicals production, where sustainable alternatives to traditional chemical synthesis are sought, fermentation processes play a crucial role [1, 2]. These processes utilize microorganisms to convert renewable feedstocks such as sugars, starches, or lignocellulosic biomass into valuable chemicals and fuels [3, 4]. However, the presence of inhibitor compounds such as hydroquinone (HQ), 5-hydroxymethylfurfural (HMF), furfural (FF), and vanillin (VAN) in fermentation broth poses a significant challenge to the efficiency and productivity of these processes [5, 6]. The inhibitor substances present in the fermentation broth not only impede the development of microorganisms but also hinder their capacity to produce desired chemicals and fuels [7].

In order to minimize the adverse impacts of inhibitory compounds, it is crucial to devise efficient separation techniques for isolating these inhibitors from the fermentation broth [8]. Traditional methods such as membrane extraction [9, 10], membrane filtration [11, 12], solvent extraction [13, 14], ion-exchange [15, 16], and the genetic modification of fermenting microorganisms [17, 18] often suffer from low efficiency, high cost, or environmental concerns [4, 19].

Among these methods, liquid-liquid extraction (LLE) has gained attention due to its simplicity, cost-effectiveness, safety, and potential for nearly complete removal of inhibitory compounds from hydrolysates. Recently, deep eutectic solvents (DES), a new class of "green solvents," have attracted interest due to their low toxicity, cheap synthesis, and high biodegradability. DES, consisting of two or more compounds forming eutectic liquids via interactions between hydrogen bond donors (HBD) and acceptors (HBA), have garnered attention in green and sustainable chemistry [20]. Although, ionic liquids face industrial limitations such as high viscosity, difficult

recovery, and low yield and selectivity, but by integrating ionic liquids into MOFs can mitigate these issues by combining the advantages of both structures.

MOFs represent a category of crystalline materials that arise from the self-assembly of metal ions and organic ligands [21, 22]. MOFs, renowned for their extraordinary porosity, high surface area, and tunable chemical functionality, have emerged as exceptional adsorbents for a wide range of pollutants such as heavy metals [23], antibiotics [24], dye [25] and radionuclide contaminants [26]. In particular, aminated MOFs have shown great potential due to their high surface area, tunable pore structures, and chemical stability [21, 27-29]. The presence of several functional groups in MOFs provides considerable benefits in terms of surface functionality. Functionalized MOFs can be created by post-synthetically modifying organic struts and clusters with new species, providing advantages compared to their original MOFs.

Zr-based MOFs, particularly the UiO-66 (UiO stands for the University of Oslo) series, have attracted a lot of attention because of their large surface area, great thermal and chemical stability, and low toxicity [30, 31]. The remarkable stability of this family of materials has been demonstrated throughout a broad spectrum of temperature, pressure, pH, and humidity levels. This class of materials has a cubic close-packed unit cell structure and is based on $Zr_6O_4(OH)_4$ octahedral nodes [32, 33]. Terephthalic acid-based linkers build lattices by connecting nodes 12 times. Their high chemical and thermal stability can be attributed to strong affinity of oxygen linkers for zirconium's. Reactive functional groups must occasionally be added to this family of materials to customize it for certain hazardous chemical mitigation applications, despite its inherent versatility. In other words, by introducing reactive functional groups, the intrinsic adaptability of MOFs like NH_2-UiO-66 can be modified for applications involving the mitigation of hazardous chemicals. These alterations improve the material's capacity to interact with and

sorption different contaminants, therefore expanding its usefulness in environmental cleanup. As mentioned previously; to overcome the problems of ionic liquids, they can be combined with MOFs, hoping to combine the advantages of both materials into something new and more effective. Cheng et al. [34] describe the preparation of UiO-66 of Zirconium based metal–organic frameworks through DESs with controlling over the particle size and defects to improve the adsorption of PFASs. For the quantitative analysis of the structural properties of the synthesized materials, the study employed carrying out analyses including; SEM, FTIR, and XRD analyses. The adsorption kinetics indicated that in the case of this experiment, it took roughly 100 minutes to get to equilibrium and as early as 40 minutes, 90% of the PFAS had been adsorbed. The study also revealed a relationship between the degree of defect and the adsorption capacity of the material; however, the authors pointed out that small crystals and high defect rates do not automatically translate into improved results, which underscores the dependency of the efficiencies of the structural characteristics of the highly complicated relationship. One has to appreciate that the research outcomes of DES-based UiO-66 materials affirmed the role of these materials in environmental application including, but not limited to, decontamination of water from PFAS groups. Additionally, Liu et al. [35] conjured three DES-functionalized adsorbents, namely, ZMG-BA, ZMG-FA, and ZMG-PA. The modification of the materials for having other absorption sites enhanced the selectivity and efficiency of chemically selective capture and the recyclability of the materials. The system of hydrogen bonding seemed to be interactive according to the results of the DFT models as well as FTIR and XPS experiments. Further knowledge regarding these materials was gained to experimental and theoretical approaches. The ZMG-BA adsorbent was the most efficient, removing amphetamine (AMP) at 91.06%. ZMG-FA and ZMG-PA followed with removal rates of 79.56% and 70.73%, respectively, while non-functionalized

ZMG had the lowest rate at 61.34%. As far as the collection of AMP from water is concerned, DES-functionalized adsorbents, especially ZMG-BA, useful. The work elucidates on how these materials operate; most importantly, hydrogen bonding, and points to the potential of the materials in applications such as environmental remediation.

This work focuses on the preparation of ChCl@NH_2-UiO-66 by the direct in situ formation of a highly stable interaction between the MOF and choline chloride. In the synthesis process, the −NH_2-functionalized UiO-66 was mixed with choline chloride (ChCl) at thermal and solvent-free conditions to give ChCl@NH_2-UiO-66. To date, the use of UiO-66-MOPO as an intermediate for synthesizing MOFs with DESs, UiO-66 incorporated NH_2 groups as hydrogen donating species and ChCl as hydrogen accepting species creating an in-situ DES within the MOF structure. This interaction increases the adsorption capacity of the material for inhibitory compounds thus a proper method for the removal of these compounds from different samples.

The aim of this study is to synthesize a new MOF@DES composite using (NH_2-UiO-66) MOF and DES (ChCl) structures to remove FF, HMF, HQ, and VAN from the broth after hydrolysis and the waste after fermentation samples. After optimization of pH, temperature, stirring speed, volume of sample solution, contact time, and the amount of ChCl@NH_2-UiO-66, it was applied to real samples for the efficient removal of the phenolic inhibitory compounds. To achieve optimal conditions for this removal process, the Box-Behnken design (a statistical method for response surface methodology) was employed to systematically optimize the variables involved in the extraction process, ensuring maximal efficiency and effectiveness. Box-Behnken design on the other hand can be describe as a very efficient statistical design tool for response surface methodology since it is well suited for optimizing processes with more than two variables [36, 37]. In this work, it also used for the systematic study of the major factors like pH, temperature and

contact time for getting the best efficiency of the removal of the inhibitory compounds by the ChCl@NH_2-UiO-66 sorbent. This strategy enabled the reduction of the number of experimental runs while at the same time covering enough area of the interaction of the taken variables in order to find out the best conditions to operate under. This is a new and novel method for this purpose, and so far, this sorbent has not been used to remove inhibitor compounds derived from biomass hydrolysis.

2. Experimental

2.1. Reagents

Zirconium (IV) chloride ($ZrCl_4$, purity ≥99.5%), 2-aminoterephthalic acid (NH_2-BDC, 99%), choline chloride (ChCl, ≥98%), hydrochloric acid (HCl ≥38%), and sodium hydroxide (NaOH, ≥99%), and acetic acid (purity ≥98%), were obtained from Sigma-Aldrich (MO, USA). Dimethylformamide (DMF, ≥99%), and ethanol (EtOH, ≥98%) were purchased from POCH company. 5-hydroxymethylfurfural (HMF, ≥99%), furfural (FF, ≥99%), hydroquinone (HQ, ≥99%), and vanillin (VAN, ≥99%) were purchased from Chemat (Gdańsk, Poland).

2.2. Apparatus

Powder X-ray diffraction (PXRD) data were collected using a Rigaku MiniFlex 600 Benchtop X-ray diffractometer from Japan equipped with a Cu Kα radiation source (λ=0.154 nm) in the range of 2-40° (step 1°. min^{-1}). Fourier-transform infrared spectroscopy (FT-IR) characterizations of the surface functional groups of MOF and MOF-DES nanomaterials were performed by a Thermo Scientific Nicolet iS50 FTIR spectrometer (USA) at room temperature at the wavenumber range of 650–4000 cm^{-1}. The Scanning Electron Microscope (SEM, FEI Quanta FEG 250, USA) with the energy-dispersive X-ray spectroscope (EDX, EDAX Genesis APEX 2i, USA) and Apollo

X SDD detector were used. SEM analysis was performed using the secondary electrons (SE) detector at 10 kV of accelerating voltage. Thermogravimetric analysis (TGA), for investigating thermal stabilities, was conducted under a nitrogen atmosphere using a Mettler Toledo TGA2 instrument (USA) at a dynamic mode from room temperature to 800°C with a heating rate of 10°C min^{-1}. This apparatus operates autonomously calculate derivative thermogravimetry (DTG) curves by STARe Software. The Brunauer-Emmett-Teller (BET) method was used to determine the specific surface area using a Micromeritics Gemini V200 Shimadzu analyzer (Japan). The specific surface area was evaluated by a multipoint method using the adsorption data for a relative pressure (p/p_0) range of 0.05–0.3.

To analyze phenolic inhibitors using chromatography, a Merck Hitachi high-performance liquid chromatography (HPLC) system from Germany was utilized, featuring a diode array detector (Beckman Coulter, USA, model DAD 166). The analytical column employed was a C18 column (250 mm × 4.6 mm, with 3 μm particles). The mobile phase, comprising water: methanol: acetonitrile in a ratio of 88:4:8 v/v%. The elution was isocratic at a flow rate of 0.6 $mL.min^{-1}$. The detector operated at an analytical wavelength of 284 nm, and the column temperature was maintained at room temperature. The HPLC analyses are presented in Figs. S1-S3.

The ATR-FTIR spectroscopy was performed to study the process of inhibitors sorption, as depicted in Figs. S4-S8. The FTIR analysis was performed using OPUS software from Bruker, USA, on a Bruker Tensor 27 spectrometer equipped with an ATR accessory. Spectra were recorded in the spectral range from 4000 to 1000 cm^{-1}, 256 scans for both background and sample, with resolution 4.5 cm^{-1}, and slit width 0.5 cm.

The removal efficiency (RE%) of the inhibitors was determined by applying Eq. 1:

$$RE\ (\%) = \frac{C_i - C_f}{C_i} \times 100 \quad (1)$$

Here, C_i represents the initial concentration, and C_f denotes the residual concentration of inhibitors both measured (mg. L^{-1}) respectively.

2.3 Procedures

2.3.1 Synthesis of NH_2-UiO-66

NH_2-UiO-66 was synthesized according to Li et al. reported procedure [38]. In a 250 ml laboratory glass bottle, $ZrCl_4$ (1.7 mmol) in DMF (50 mL) was stirred at 50–60°C for 10 min. 2-amino terephthalic acid (1.7 mmol) was then added to this solution and stirred for 10 min, after which the mixture was heated at 120 °C for 24 h in the oven. After that, the solution was cooled down to room temperature, and the solid was collected by filtration, washed with DMF (2 times), and then ethanol (4 times). Lastly, the MOF were dried (90 °C, 3 h, under vacuum condition) to give the $Zr_6O_4(OH)_4$ $(BDC\text{-}NH_2)_6$. After the drying step, MOF was soaked in ethanol 3 times, each time using 10 mL of ethanol, to exchange the guest molecules from pores. The material was isolated by decanting, and the powder was heated at 150°C under vacuum conditions overnight to remove the solvent and humidity prior to further analyses and use.

2.3.3. Integration of deep eutectic solvent into NH_2-UiO-66 (ChCl@NH_2-UiO-66)

The procedure was initiated by combining 50 mg of MOF and 31 mg of ChCl in a test tube, followed by magnetic stirring at 80 °C for 4 hours [39]. Subsequently, the mixture was cooled to room temperature, resulting in the formation of a dark yellow solid.

2.3.4. Preparation of Real sample

To obtain hydrolysates with a high concentration of fermentable sugars, a process of breaking down lignocellulosic raw materials was conducted. A mixture of hardwoods, including beech, energetic willow, and poplar, underwent laboratory drying at 105°C for approximately 2-3 days. Potato peel and a solution containing remaining starch were also used as real samples rich in both polysugars, starch, and lignocellulose. The goal was to produce hydrolysates rich in sugars suitable for subsequent fermentation. The pre-treatment of biomass involved the use of three different reagents: sulfuric acid, sodium hydroxide, and hydrogen peroxide.

Specifically, samples were prepared by combining 3.0 g of the tested biomass with 20 mL of the specified catalyst. Each hydrolysis sample was then treated with 20 mL of either sodium hydroxide solution, sulfuric acid, or hydrogen peroxide, each with a specific concentration. The samples were hermetically sealed by double-taping and placed in a laboratory shaker, maintained at 60°C with a rotation speed of 100 rpm for 40 hours. The same procedure was repeated for all catalysts to create blank samples. Following the specified hydrolysis duration, the samples were taken out of the shaker and subjected to centrifugation for the purpose of separating the sediment. The resultant solution was filtered through a 0.45 μm PTFE syringe filter and promptly stored at -80°C for subsequent analysis.

2.4 Sorption processes

In order to remove HMF, FF, HQ, and VAN, the pH of 2 mL sample solutions was adjusted to 4. Subsequently, 8 mg of ChCl@NH_2-UiO-66 was introduced, and the resulting mixture was vortexed for 15 min. Prior to conducting the analysis, the samples were filtered using a syringe filter containing a 0.22 μm Nylon membrane. Following the filtration, 30 μL of the resulting liquid sample was introduced into the HPLC system. The obtained values were then compared with the initial concentrations, and the efficiency of sorption was computed.

3. Results and discussions

3.1. Characterization of the ChCl@ NH_2-UiO-66

The NH_2-UiO-66 metal-organic framework (MOF), which is based on zirconium, was synthesized using solvothermal methods. It was then modified by including a DES consisting of choline chloride (ChCl) and urea. This alteration was intended to improve the functional features of the MOF for potential use in mitigating dangerous chemicals. The effective synthesis and modification of ChCl@NH_2-UiO-66 were verified by several characterization approaches, which will be elaborated upon in the subsequent sections.

3.1.1. XRD

The formation of NH_2-UiO-66 structure was confirmed by powder X-ray diffraction, and the relevant patterns are presented in Fig. 1. The X-ray diffraction (XRD) investigation shown in Fig. 1 provides important information about the crystallinity and structural integrity of NH_2-UiO-66 and its choline chloride modified variant, ChCl@ NH_2-UiO-66. The diffraction peaks at 7.2°, 8.3°, 11.8°, 13.9°, 14.6°, 16.8°, 18.4°, 18.9°, 20.7°, 22.0°, 25.0°, 25.5°, and 30.5° correspond respectively to (111), (200), (220), (311), (222), (400), (331), (420), (422), (511), (531), (600), and (711) Bragg planes of the octahedral crystals which is in agreement with other studies on NH_2-UiO-66 (COD - 4348132) [38-40]. Given their effect on MOF performance in applications, these peaks' sharpness and intensity imply a high degree of crystallinity and excellent order within the crystal lattice. The ChCl@NH_2-UiO-66, XRD results showed no shifts or change in peaks intensity and confirming that NH_2-UiO-66 were structurally stable after the postsynthetic modification.

3.1.2. FTIR

Fig. 2 presents the FTIR spectroscopy analysis, which offers important information about the chemical composition and changes in functional groups of NH_2-UiO-66 and its modified version, ChCl@NH_2-UiO-66. The peaks at 3482 and 3387 cm^{-1} correspond to the N-H asymmetric and symmetric stretching vibrations confirming the presence of primary amine in NH_2-UiO-66. The N-H wiggling band observed at ~764 cm^{-1} can be also attributed to the presence of the amine group in the linker. The vibration bands at 1695, 1579, 1494, 1388, and 1258 cm^{-1} correspond to the stretching modes of C=O, O-C=O (asymmetric carboxylate), C=C, O-C=O (symmetric carboxylate), and Caromatic-N bonds [38, 39]. The band at 664 cm^{-1} corresponds to the stretching mode of μ_3−O in Zr-O-Zr, central to the MOF structure [41]. NH_2-UiO-66 undergoes post-synthetic alteration with choline chloride, resulting in additional ChCl bands at 3012, 1156, 1180, and 865 cm^{-1}. These bands correspond to the asymmetric bending of -OH (suggesting interaction or modification involving hydroxyl functions), rocking CH_2, asymmetric stretching of CCO (indicating the incorporation of ChCl's molecular structure into the framework), and stretching NCH_3 (a direct signature of the choline component in the framework) [42]. Fig. 2 shows that the absorption band of NH_2-UiO-66 at 3287 cm^{-1} shifts to 3419 cm^{-1} and broadens. This attributes to the strong hydrogen bonds produced between NH_2-UiO-66 and ChCl. These findings point to effective NH_2-UiO-66 alterations that lead to the production of ChCl@NH_2-UiO-66 [43]. The FTIR spectrum of ChCl also has different peaks to give more information for the changes of ChCl@NH_2-UiO-66 sample. The characteristic bands present in ChCl should stand out from those accompanying the MOFs before and after the biofunctionalization process to determine ChCl's chemical integration into the MOF structure. These include the appearance of new bands or variations in the position and broadening of bands that are characteristic of ChCl in the spectrum of the modified MOF NH_2-UiO-66.

3.1.3. SEM

SEM was also used to examine the morphology, shape, and size of NH_2-UiO-66, and ChCl@NH_2-UiO-66 (Fig. 3a–f). The pictures revealed that the pristine NH_2-UiO-66particles exhibit octahedral shape with sizes ranging from 100 to 200 nm due to its octahedral ZrO_6 nodes and organic linker arrangement in the crystal structure (Fig. 3a-c) [44]. Furthermore, the integration of MOF with ChCl produces the ChCl@NH_2-UiO-66, a deep eutectic solvent over the NH_2-UiO-66, as shown in Fig. 3d-f. However, there were subtle surface modifications and changes in the particle aggregation state due to the presence of ChCl. Following that, energy dispersive X-ray (EDX) analysis of the NH_2-UiO-66and ChCl@NH_2-UiO-66 indicated that the presence of nitrogen (N), oxygen (O), and zirconium (Zr), which is consistent with its chemical composition of Zr nodes linked by nitrogen-containing organic linkers. According to these results, the chemical composition of the MOF is as follows: N (22.10 wt%), O (42.34 wt%), Zr (35.56 wt%), and the composition of ChCl@NH_2-UiO-66 is as follows: N (14.66 wt%), O (22.25 wt%), Zr (14.12 wt%), and Cl (6.65 wt%). Obtained results validate the effective post synthetic alteration (Fig. 4) and prove that ChCl was successfully incorporated into the framework, through the pores or on the surface of the MOF particles. Furthermore, elemental mapping pictures of the corresponding MOF indicated that all elements (particularly Cl) were evenly distributed throughout the framework [39]. Overall, the reported findings from SEM and EDX investigations are consistent with what is predicted from effective ChCl integration into a MOF framework. The constant particle morphologies of NH_2-UiO-66 and ChCl@NH_2-UiO-66 indicate that the addition of ChCl does not jeopardize the structural integrity of the original MOF framework. Instead, the presence of ChCl may improve its features, such as its ability to interact with other chemicals. These thorough data from SEM and EDX analysis demonstrate not only structural preservation after alteration, but also

the successful integration of the deep eutectic solvent, thus opening up new paths for specialized uses of this MOF material.

3.1.4. TGA

Thermogravimetric analysis was used to test the thermal stability of MOF, as shown in Fig. 5 for NH_2-UiO-66 and ChCl@NH_2-UiO-66. For both samples, the first mass loss between 100°C and 150°C was caused by the removal of physically adsorbed water and DMF which are used in the synthesis process trapped in the pores of the NH_2-UiO-66 and ChCl@NH_2-UiO-66. Between 200°C and 380°C, NH_2-UiO-66 lost 20% of mass due to dihydroxylation of the $[Zr_6O_4(OH)_4]^{12+}$ nodes. Mass loss between 380°C and 550°C was attributed to the thermal decomposition of 2-aminoterephthalic acid ligand, thereby the breakdown of NH_2-UiO-66, resulting in the production of ZrO_2. In addition, the ChCl@NH_2-UiO-66 revealed two different mass loss areas between 200 and 550°C. At temperatures ranging from 200 to 260°C, mass loss of about 35 % could be attributed to Zr_6 node dehydroxylation. At temperatures ranging from 260°C to 550°C, mass loss of approximately 42 wt% could be attributed to DES component breakdown and MOF framework cleavage [39]. The effects of dysfunctioning of the DES component led to even more changes of the structure and leads to the disintegration of the MOF framework. Mass loss is remarkably higher in case of NH_2-UiO-66 with ChCl exposed to temperature between 260 to 360ºC compared to NH_2-UiO-66 alone, which itself suggest that ChCl play a crucial role in modifying thermal characteristics and degradation profile of the MOF. From the TGA curve of the ChCl sample, it is possible to obtain a clear and definite TGA profile for thermal degradation. Despite this Aller difference, which onset of ChCl decomposition can be assumed to be at about 300°C based on the conspicuous disappearance of mass at around this temperature. Furthermore, the mass loss is an ongoing process as temperature increases and this leads to the disintegration of ChCl into

individual components. This reaction clearly shows that, ChCl is thermally less stable than the MOF samples because it starts to decompose at lower temperature. Thus, the general understanding of the TGA analysis is given to depict the thermal stability and some degradation processes of NH_2-UiO-66, ChCl, and ChCl@NH_2-UiO-66. The first weight loss due to the evaporation of volatile compounds, and weight loss due to the dehydroxylation, dissociation of ligands from the metal center, and disintegration of DES component demonstrate the rather complex thermal characters of these molecules. The presence of ChCl in the MOF structure influences the thermal stability and the breakdown pathways and hence the overall difference in the incidence of mass loss with the unmodified MOF. An overview of thermal degradation is thus important for enhancement of the thermal performance of MOFs in their intended use.

3.1.4. Surface area (BET)

Specific surface area measurements indicated that ChCl@NH_2-UiO-66 is prominently porous with a Brunauer-Emmett-Teller (BET) surface area of 344 m^2g^{-1} (Fig. 6). The decrease trend in BET surface area from 778 m^2g^{-1} for NH_2-UiO-66 to 344 m^2g^{-1} for ChCl@NH_2-UiO-66 is due to the formation of NH_2 linkages (formation of hydrogen bonds between the NH_2 groups on NH_2-UiO-66 and the hydroxyl groups of choline chloride (ChCl)) with ChCl toward synthesis of the ChCl@NH_2-UiO-66 [39, 45].

3.2. Box Behnken design

Box Behnken Design (BBD) is a statistical plan that allows design of experiment with respect to simultaneous variation of all experimental factors. BBD is frequently applied to determine the optimum values of various process conditions during analytical processes. In the BBD model, all the experiments run according to predefined range of parameters. Four explanatory variables were

taken into account on 3 levels, so 27 experiments are required to be carried. A list of process parameters is presented in Table S1 along with the adopted levels.

In this study, the BBD model was used to evaluate the effect of four variables (i.e. vortex time, pH, concentration of analyte, and adsorbent amount) and their effect on RE of FF, HMF, HQ and VAN. The selected parameters were chosen based on previous studies [46, 47]. The extended values for all are presented in Table S1. The design matrix, as well as experimental and model-predicted responses for RE of FF, HMF, HQ and VAN are listed in Table S2.

The analysis of variance (ANOVA) was used to select the statistically important interactions and effects of the variables on FF, HMF, HQ and VAN RE from aqueous model samples. The ANOVA test results are presented in Table S3. The p- and F-values were set at a 95% confidence level in the ANOVA test. Only the parameters and interactions with p-value less than 0.05 were considered as statistically significant and influential on the BBD model. Obtained results allowed to calculate polynomial quadratic models for selective RE of HMF. FF. HQ and VAN (Eqs. 2-5) and universal removal of all tested substances (Eq. 6):

$$Y_{HMF} = -2 + 6.67\,X1 + 5.0\,X2 - 2.6\,X3 + 5.9\,X4 - 0.402\,X1 \times X1 - 1.07\,X2 \times X2 + 0.169\,X3 \times X3 - 1.345\,X4 \times X4 + 0.189\,X1 \times X2 - 0.360\,X1 \times X3 + 0.319\,X1 \times X4 + 0.39\,X2 \times X3 - 0.07\,X2 \times X4 + 0.806\,X3 \times X4 \quad (2)$$

$$Y_{FF} = -55.6 + 10.50\,X1 + 8.2\,X2 - 5.31\,X3 + 9.18\,X4 - 0.129\,X1 \times X1 - 0.61\,X2 \times X2 + 0.337\,X3 \times X3 - 0.646\,X4 \times X4 - 0.741\,X1 \times X2 - \quad (3)$$

$$0.320\,X1 \times X3 - 0.312\,X1 \times X4 + 0.958\,X2 \times X3 - 0.02\,X2 \times X4 + 0.200\,X3 \times X4$$

$$Y_{HQ} = -55.5 + 1.69\,X1 + 19.3\,X2 - 1.08\,X3 + 6.51\,X4 + 0.015\,X1 \times X1 - 0.94\,X2 \times X2 - 0.306\,X3 \times X3 + 0.114\,X4 \times X4 - 0.611\,X1 \times X2 + 0.615\,X1 \times X3 - 0.262\,X1 \times X4 + 0.073\,X2 \times X3 - 0.163\,X2 \times X4 - 0.539\,X3 \times X4 \quad (4)$$

$$Y_{VAN} = -83.9 + 1.77\,X1 + 23.5\,X2 + 1.38\,X3 + 26.74\,X4 - 0.326\,X1 \times X1 - 1.33\,X2 \times X2 - 0.293\,X3 \times X3 - 0.438\,X4 \times X4 + 0.425\,X1 \times X2 + 0.667\,X1 \times X3 - 0.336\,X1 \times X4 - 0.204\,X2 \times X3 - 2.291\,X2 \times X4 - 0.896\,X3 \times X4 \quad (5)$$

$$Y = -197 + 20.6\,X1 + 56.1\,X2 - 7.6\,X3 + 48.3\,X4 - 0.843\,X1 \times X1 - 3.95\,X2 \times X2 - 0.094\,X3 \times X3 - 2.32\,X4 \times X4 - 0.74\,X1 \times X2 + 0.602\,X1 \times X3 - 0.590\,X1 \times X4 + 1.22\,X2 \times X3 - 2.55\,X2 \times X4 - 0.428\,X3 \times X4 \quad (6)$$

The analysis of results allows to conduct. that it is possible to carry the process with process parameters that promote a selective removal of one of the tested substances or a universal removal. in order to remove all the substances with significant efficiency. In the further part of experiment. the model will be applied to remove defined substances from real post-fermentation broths. The optimal values of selective and universal process parameters shall be applied according to Table 1.

Both approaches allow to obtain relatively high determination coefficient equal to 0.81 (HMF), 0.84 (FF), 0.79 (HQ), 0.93 (VAN), 0.79 (universal) respectively. In addition, the predicted determination coefficient and adjusted determination coefficient (Table S3) were obtained with satisfactory values. This indicates the proper correlation between the experimental and model-predicted results and good model fitting in the tested range. Based on the results, it assumed, that new data can be predicted within the model, however comparison with real samples is required, as diversified derivative substances may be present in the solutions and affect the efficiency of removal of tested substances.

The surface plots of BBD obtained according to Eqs 2-6 are presented in figs. S9-S13. Surface plots graphically illustrate the interactions of individual variables with each other and assess their impact on the efficiency of HMF, FF, HQ and VAN removal. Only the results which represent positive values of inhibitors concentrations as model-predicted values are presented, since only positive values can be considered as results corresponding with the experiment course.

In diagram 7, one can observe the mutual effects of variables X1 and X2 (Fig. S9a) and X1 and X4 (Fig. S9b). Based on the course of the response surface area, it can be observed that in the tested range of variability an increase in the model-predicted HMF sorption efficiency can be observed. Similarly, the interplay of variables 1 and X2 (Fig. S10a) and X1 and X4 (Fig. S10b) affects the FF sorption efficiency. For these chemicals, adsorption efficiency is expected to increase with increasing adsorbent mass fraction and increasing vortex time. It should be noted that in the case of HMF the response surface area is located at the central point of the distribution, while for FF it is slightly shifted to the right, which suggests that the actual values of the optimal parameters may be close to the experimental limit. In order to identify conditions under which the sorption efficiency of FF and HMF can be selectively increased, the scope of the experiment should

be expanded. In the case of HQ adsorption, the mutual effects of variables such as X1 and X2 (Fig. S11a), X2 and X3 (Fig. S11b), X2 and X4 (Fig. S11c) allow it to be clearly stated that increasing such elements as the initial pH and the mass share of the adsorbent while reducing the analyte concentration have a positive effect on the sorption efficiency. This information is valuable from a technical point of view and justifies the applicability of the method for solutions with low HQ concentrations. Considerations regarding the VAN sorption efficiency revealed (Fig. S12) that the mutual influence of pH and the mass fraction of the adsorbent significantly influence the increase in sorption efficiency. It should be noted that the highest yields were achieved at no pH with a simultaneous high share of adsorbent. An experiment was also carried out to identify sorption conditions for which all tested substances were efficiently adsorbed simultaneously (Fig. S13). It was found that high yields are obtained for specific combinations of variables X1 and X2, i.e. similarly to the sorption of HMF, FF and HQ. However, in the case of sorption promoting the removal of all substances at the same time, it turned out to be most beneficial to use average values of vortex time and pH in the tested variability range. Similarly, the interplay of X2 and X4 enables high sorption efficiencies, theoretically exceeding 100%, when a high adsorbent ratio is used at low pH.

In the next part of the study the BBD models were tested under real conditions. Samples of lignocellulosic biomass hydrolysates and post-fermentation broths were used for HMF, FF, HQ and VAN removal. The characteristics of real samples is provided in Table 2.

Table 2 shows the results describing the sorption efficiency described by the method from real samples. Lignocellulosic waste and its alkaline, acidic and oxidative hydrolysis hydrolysates using low and high concentrations of hydrolysis catalysts were used as actual samples. The sample type is shown in the 'sample origin' column. The selection of real samples is dictated by actual processes

carried out in a separate experiment, in which waste streams containing the tested substances are created. sorption using MOF was proposed as a stage enabling the management of these waste streams. Since the samples used are real, it is not possible to control the content and concentration of the tested substances. However, since the method used took into account the amount of adsorbent, it is assumed that the mutual proportions of X3 and X4 will enable the determination of possible adsorption efficiencies. In the case of samples 1.1 and 1.2, i.e. hardwood blend samples obtained by acid hydrolysis and samples 1.3 and 1.4 obtained by alkaline hydrolysis, the formation of high HQ concentrations during hydrolysis is observed. At the same time, the use of the sorption method described by the optimal values of the dependent variables allows for the removal of HMF and VAN with the highest efficiency, if any are present in the sample. In the case of HQ removal, the yields recorded in Table 2 are lower, but it should be remembered that quantitatively the concentrations of these substances are higher in the input samples. In samples 1.5 and 1.6, i.e. hardwood blend samples after oxidative hydrolysis, the leading by-product identified in the liquid is HMF. Its sorption efficiency remains at the level corresponding to other hydrolysates (samples 1.1-1.4). sorption from samples 2.1, 2.4 and 2.5 obtained as a result of alkaline, oxidative and acidic treatment of lignocellulosic waste from corn cobs, respectively, reveals that in this type of bulk mass there are low HQ contents, with relatively high HMF concentrations (2.2-2.5). However, it is possible to remove HMF with an efficiency of even more than 62%. At the same time, it is stated that it is possible to remove all tested components under non-selective conditions (described as Y in Table 1). Similar effects were observed for starch and lignocellulose hydrolysate from potato peel processing after centrifugation and after acidic and alkaline pre-treatment (1.7-1.9). In the case of biomass containing starch, a decrease in the removal efficiency of the tested substances compared to the mixtures was observed, which may be due to the presence of additional substances

that were not detected for lignocellulose-based biomass, which are also secondary products of the transformation of mono- and disaccharides originating from starch, which may undergo secondary transformations in the presence of acids and bases.

3.3. Effects of matrix composition in real samples treatment

In order to assess the efficiency of the newly developed method, the conducted removal experiments under optimal conditions using real samples obtained after hydrolysis and fermentation. Table 2 illustrates the results of the RE of inhibitor compounds. As demonstrated in this table, the RE of HQ, HMF, FF, and VAN in real samples after hydrolysis and fermentation exceeded 51.73%, 53.21%, 42.69%, and 37.59%, respectively. These results unequivocally showcase the effectiveness of employing ChCl@NH_2-UiO-66 for eliminating these inhibitory compounds from hydrolyzed and fermented samples.

The lower RE observed in hydrolyzed and fermented samples using the ChCl@NH_2-UiO-66 method compared to synthetic samples can be attributed to several factors. Real samples obtained after hydrolysis and fermentation contain a complex matrix with a variety of organic components. These matrix components can interfere with the removal process by competing for sorption sites or altering the chemical interactions between the inhibitory compounds and the ChCl@NH_2-UiO-66. On the other hand, other substances present in real samples, which contain the -OH or -COOH group in their chemical compositions, can form connections with the ChCl@NH_2-UiO-66 through hydrogen bonding or van der Waals interactions [4, 7, 48, 49]. These interactions may obstruct the active sites in the ChCl@NH_2-UiO-66 and restrict the effectiveness of inhibitory compound removal. Therefore, the RE in real samples was lower than in synthetic samples.

3.4. Comparison of ChCl@NH_2-UiO-66 *with* NH_2-UiO-66

Fig. 7, shows the performance of ChCl@NH_2-UiO-66 and NH_2-UiO-66 for the removal of inhibitory compounds. From the table, a high difference in the performance is appreciated. In the actual sense, ChCl@NH_2-UiO-66 composite had far higher RE of the inhibitory chemicals than MOF. The reasons for the improved reactivity of molecules such as HQ, HMF, FF, and VAN are several in terms of their interaction with ChCl@NH_2-UiO-66. Incorporating Choline Chloride into the MOFs introduces functional groups of hydroxyl (-OH) and chloride (Cl-); that is, it enhances the propensities toward interactions with other chemicals by hydrogen bonding and electrostatic interactions. Second, the presence of ChCl further increases the hydrophilic nature of MOF surfaces, which thus leads to an increase in the compatibility of MOF with polar molecules like HQ, HMF, FF, and VAN. The combination of MOFs with ChCl seems to display a kind of synergistic effect in the overall system. This increases the performance because there is an increase in stability, chemical interaction, and selectivity. In the application of this material, approximately ChCl, the rate of adsorption increased, and thus, it was influential in removing the component.

3.5. Reusability

The reusability of MOF@DES while maintaining its original characteristics is crucial for both conserving resources and achieving economic benefits. Based on optimized conditions, as shown in Fig 8, ChCl@NH_2-UiO-66 demonstrates reusability for up to four cycles without significant reduction in the RE of inhibitors. This reusability indicates that ChCl@NH_2-UiO-66 maintains its functional properties after repeated use. However, after the fourth cycle, a noticeable decline in RE becomes apparent, suggesting that the material's capacity to effectively target and eliminate inhibitory compounds begins to diminish. These results emphasize the impressive initial capacity and reusability of ChCl@NH_2-UiO-66, positioning it as an efficient method for inhibitor removal.

3.6. Mechanism of sorption

The mechanism of inhibitory compound sorption by ChCl@NH_2-UiO-66 is detailed in Section S.2 of the supplementary material. (Figs. S4-S8)

3.7. Comparison with other methods

The comparison of the ChCl@NH_2-UiO-66 method with other techniques for the removal of inhibitory compounds from hydrolysates is described in section S.4 and table S4 of the supplementary materials.

4. Conclusions

The utilization of ChCl@NH_2-UiO-66 has demonstrated high effectiveness in removing inhibitory compounds from fermentation broth. Under optimum conditions (pH 5.8, concentration 9 ppm, vortex time 11 min and amount of ChCl@NH_2-UiO-66 5mg) the RE of 62.08%, 56.09%, 45.29%, and 83.46% were achieved for HQ, HMF, FF, and VAN, respectively. However, the RE of real samples after hydrolysis and fermentation for HQ, HMF, FF, and VAN were lower, with values of 51.73%, 53.21%, 42.69%, and 37.59%, respectively. The lower RE of inhibitory compounds in hydrolyzed and fermented samples using the ChCl@NH_2-UiO-66 method compared to synthetic samples can be attributed to the complex matrix composition, chemical interactions with matrix components, and variations in sample composition. XRD, TGA, DSC, FTIR, BET, SEM, and EDX were used to characterize the catalysts and evaluate the impact of choline chloride on NH_2-UiO-66. The addition of choline chloride to NH_2-UiO-66 resulted in changes observed in FTIR, BET, EDX, and FESEM analyses, confirming the synthesis. In conclusion, ChCl@NH_2-UiO-66 demonstrates significant advantages in the removal of inhibitor compounds from hydrolysis and fermentation broths. The mechanism of removing inhibitor compounds by ChCl@NH2-UiO-66 involves hydrogen bonding and electrostatic interactions between N–H and carboxylate groups in the MOF with the functional groups of inhibitors, van der

Waals forces with aliphatic C–H groups, and π-π stacking interactions between aromatic rings. Therefore, with its high effectiveness, versatility, and robust removal capabilities, the ChCl@NH_2-UiO-66 offers a promising solution for removing inhibitory compounds.

CRediT authorship contribution statement

Zhila Honarmandrad: Writing – original draft, Methodology, Investigation, Data curation. Seyed Soroush Mousavi Khadem: Writing – original draft, Synthesis, Characterization. Karolina Kucharska: Formal analysis, Resources, Methodology, Writing - Review & Editing. Massoud Kaykhaii: Writing – review & editing. Justyna Łuczak: Writing – review & editing, Jacek Gębicki: Writing – review & editing, Funding acquisition.

Declaration of competing interest

The authors declare that they have no known competing financial interests or personal relationships that could have appeared to influence the work reported in this paper.

Author contributions

ZH: did the practical work and prepared the manuscript, SSMK: did the practical work and prepared the manuscript, KK: provided and prepared the real samples. KK, MK, JŁ and JG planned the study and wrote the manuscript. All authors read and approved the final manuscript.

Data availability

The majority of the data used to support the findings of this study are included within the article. Other data are available from the corresponding author upon request.

Funding

Research is funded by the National Science Centre Poland via OPUS grant no. UMO2021/41/B/ST8/02395.

Ethics approval and consent to participate

This manuscript is the authors' own original writing, which has not been previously published elsewhere and it is not currently being considered for publication elsewhere. The authors will conduct themselves with integrity, fidelity, and honesty. They will openly take responsibility for actions, and only make agreements, which they intend to keep. The authors will not intentionally engage in or participate in any form of malicious harm to another person or animal.

References

[1] S. Liu, Bioprocess engineering: kinetics, sustainability, and reactor design, Elsevier, (2020)

[2] S.J. Malode, K.K. Prabhu, R.J. Mascarenhas, N.P. Shetti, T.M. Aminabhavi, Recent advances and viability in biofuel production, Energ. Convers. Man-X. 10 (2021).

[3] Z. Honarmandrad, K. Kucharska, J. Gębicki, Processing of Biomass Prior to Hydrogen Fermentation and Post-Fermentative Broth Management, Molecules, 27 (2022) 7658.

[4] P. Makoś-Chełstowska, K. Kucharska, E. Słupek, J. Gębicki, M. de la Guardia, Magnetic deep eutectic solvents as efficient media for extraction of furfural and 5-hydroxymethylfurfural from aqueous samples, J. Mol. Liq. 390 (2023) 122945.

[5] S. Ghosh, O. Falyouna, A. Malloum, A. Othmani, C. Bornman, H. Bedair, H. Onyeaka, Z.T. Al-Sharify, A.O. Jacob, T. Miri, C. Osagie, S. Ahmadi, A general review on the use of advance oxidation and adsorption processes for the removal of furfural from industrial effluents, Microporous Mesoporous Mater. 331 (2022) 111638.

[6] X. Meng, Y. Wang, A.J. Conte, S. Zhang, J. Ryu, J.J. Wie, Y. Pu, B.H. Davison, C.G. Yoo, A.J. Ragauskas, Applications of biomass-derived solvents in biomass pretreatment–Strategies, challenges, and prospects, Bioresour. Technol. 368 (2023) 128280.

[7] Z. Honarmandrad, K. Kucharska, M. Kaykhaii, J. Gębicki, Removal of phenolic inhibitor compounds from hydrolysates and post-fermentation broths by using a hydrophobic magnetic deep eutectic solvent, J. Environ. Chem. Eng. 12 (2024) 112621.

[8] T.A. Ewing, N. Nouse, M. van Lint, J. van Haveren, J. Hugenholtz, D.S. van Es, Fermentation for the production of biobased chemicals in a circular economy: a perspective for the period 2022–2050, Green Chem. 24 (2022) 6373-6405.

[9] D.L. Grzenia, D.J. Schell, S. Ranil Wickramasinghe, Membrane extraction for detoxification of biomass hydrolysates, Bioresour. Technol. 111 (2012) 248-254.

[10] R.K. Saini, P. Prasad, X. Shang, Y.-S. Keum, Advances in lipid extraction methods—a review, Int. J. Mol. Sci. 22 (2021) 13643.

[11] L. Pan, M. He, B. Wu, Y. Wang, G. Hu, K. Ma, Simultaneous concentration and detoxification of lignocellulosic hydrolysates by novel membrane filtration system for bioethanol production, J. Clean. Prod. 227 (2019) 1185-1194.

[12] D. Elkhatib, V. Oyanedel-Craver, A critical review of extraction and identification methods of microplastics in wastewater and drinking water, Environ. Sci. Technol. 54 (2020) 7037-7049.

[13] T.R.K.C. Doddapaneni, R. Jain, R. Praveenkumar, J. Rintala, H. Romar, J. Konttinen, Adsorption of furfural from torrefaction condensate using torrefied biomass, J. Chem. Eng. 334 (2018) 558-568.

[14] S. Ügdüler, K.M. Van Geem, M. Roosen, E.I. Delbeke, S. De Meester, Challenges and opportunities of solvent-based additive extraction methods for plastic recycling, Waste management, 104 (2020) 148-182.

[15] G.B. Carvalho, S.I. Mussatto, E.J. Cândido, J.B. Almeida e Silva, Comparison of different procedures for the detoxification of eucalyptus hemicellulosic hydrolysate for use in fermentative processes, JCTB. 81 (2006) 152-157.

[16] N.A.M. Sobri, N. Harun, M.Y.M. Yunus, A Review of the Ion Exchange Leaching Method for Extracting Rare Earth Elements from Ion Adsorption Clay, Chem. Eng. Res. Des. 208 (2024) 94-114.

[17] D. Ludwig, M. Amann, T. Hirth, S. Rupp, S. Zibek, Development and optimization of single and combined detoxification processes to improve the fermentability of lignocellulose hydrolyzates, Bioresour. Technol. 133 (2013) 455-461.

[18] P. Hanlon, V. Sewalt, GEMs: genetically engineered microorganisms and the regulatory oversight of their uses in modern food production, Crit. Rev. Food Sci. Nutr. 61 (2021) 959-970.

[19] E. Gil-Martín, T. Forbes-Hernández, A. Romero, D. Cianciosi, F. Giampieri, M. Battino, Influence of the extraction method on the recovery of bioactive phenolic compounds from food industry by-products, Food Chem. 378 (2022) 131918.

[20] C. Ferreira, M. Sarraguça, A Comprehensive Review on Deep Eutectic Solvents and Its Use to Extract Bioactive Compounds of Pharmaceutical Interest, Pharmaceuticals, 17 (2024) 124.

[21] C. Yengin, Z.P. Gumus, R. Ilktac, A. Elci, M. Soylak, Vortex-assisted solid phase extraction on MIL-101(Cr) of parabens in waters and cosmetics by HPLC–DAD, J. Iran. Chem. 20 (2023) 1383-1393.10.1007/s13738-023-02763-4.

[22] Z. Honarmandrad, M. Kaykhaii, J. Gębicki, Microplastics removal from aqueous environment by metal organic frameworks, BMC Chem. 17 (2023) 122.

[23] Q. Gao, J. Xu, X.-H. Bu, Recent advances about metal–organic frameworks in the removal of pollutants from wastewater, Coord. Chem. Rev. 378 (2019) 17-31.

[24] N. Tian, Q. Jia, H. Su, Y. Zhi, A. Ma, J. Wu, S. Shan, The synthesis of mesostructured NH 2-MIL-101 (Cr) and kinetic and thermodynamic study in tetracycline aqueous solutions, J. Porous Mater. 23 (2016) 1269-1278.

[25] Q. Yang, Y. Wang, J. Wang, F. Liu, N. Hu, H. Pei, W. Yang, Z. Li, Y. Suo, J. Wang, High effective adsorption/removal of illegal food dyes from contaminated aqueous solution by Zr-MOFs (UiO-67), Food. Chem. 254 (2018) 241-248.

[26] L. Li, W. Ma, S. Shen, H. Huang, Y. Bai, H. Liu, A combined experimental and theoretical study on the extraction of uranium by amino-derived metal–organic frameworks through post-synthetic strategy, ACS Appl. Mater. Interfaces. 8 (2016) 31032-31041.

[27] D.P. Arcon, F.C. Franco Jr, All-fatty acid hydrophobic deep eutectic solvents towards a simple and efficient microextraction method of toxic industrial dyes, J. Mol. Liq. 318 (2020) 114220.

[28] A. Dalmaz, S. Sivrikaya Özak, Green deep eutectic solvent assisted liquid–liquid microextraction procedure for Sunset Yellow dye in effervescent vitamin C tablets, J. Iran. Chem. Soc. (2022) 1-8.

[29] X. Li, K.H. Row, Development of deep eutectic solvents applied in extraction and separation, J. Sep. Sci. 39 (2016) 3505-3520.

[30] A. Jrad, P. Damacet, Z. Yaghi, M. Ahmad, M. Hmadeh, Zr-based metal–organic framework nanocrystals for water remediation, ACS Appl. Nano. Mater. 5 (2022) 10795-10808.

[31] H. Singh, A. Deep, S. Puri, M. Khatri, N. Bhardwaj, UiO-66-NH_2 MOF-based fluorescent aptasensor for detection of zearalenone in cereals, Food Control. (2024) 110497.

[32] C.A. Trickett, K.J. Gagnon, S. Lee, F. Gándara, H.B. Bürgi, O.M. Yaghi, Definitive molecular level characterization of defects in UiO-66 crystals, Angew. Chem. Int. Ed. 54 (2015) 11162-11167.

[33] O.M. Yaghi, P. Urban, L. Seungkyu, Zirconium terephthalate-based metal organic framework with open metal sites, in, Google Patents. (2023).

[34] L. Cheng, C. Fan, W. Deng, Simultaneous size and defect control of metal-organic framework by deep eutectic solvent for efficient perfluoroalkyl substances adsorption: Delving into mechanism, Chemosphere. 358 (2024) 142155.

[35] Y. Liu, S. Cao, Z. Liu, D. Wu, M. Luo, Z. Chen, Adsorption of amphetamine on deep eutectic solvents functionalized graphene oxide/metal-organic framework nanocomposite: Elucidation of hydrogen bonding and DFT studies, Chemosphere. 323 (2023) 138276.

[36] S.C. Ferreira, R. Bruns, H.S. Ferreira, G.D. Matos, J. David, G. Brandão, E.P. da Silva, L. Portugal, P. Dos Reis, A. Souza, Box-Behnken design: an alternative for the optimization of analytical methods, Anal. Chim. Acta. 597 (2007) 179-186.

[37] M.A. Bezerra, R.E. Santelli, E.P. Oliveira, L.S. Villar, L.A. Escaleira, Response surface methodology (RSM) as a tool for optimization in analytical chemistry, Talanta. 76 (2008) 965-977

[38] H. Li, H. Chu, X. Ma, G. Wang, F. Liu, M. Guo, W. Lu, S. Zhou, M. Yu, Efficient heterogeneous acid synthesis and stability enhancement of UiO-66 impregnated with ammonium sulfate for biodiesel production, J. Chem. Eng. 408 (2021) 127277.

[39] M. Akbarian, E. Sanchooli, A.R. Oveisi, S. Daliran, Choline chloride-coated UiO-66-Urea MOF: A novel multifunctional heterogeneous catalyst for efficient one-pot three-component synthesis of 2-amino-4H-chromenes, J. Mol. Liq. 325 (2021) 115228.

[40] S. Daliran, M. Ghazagh-Miri, A.R. Oveisi, M. Khajeh, S. Navalón, M. Âlvaro, M. Ghaffari-Moghaddam, H. Samareh Delarami, H. García, A Pyridyltriazol Functionalized Zirconium Metal–Organic Framework for Selective and Highly Efficient Adsorption of Palladium, ACS Appl. Mater. Interfaces. 12 (2020) 25221-25232.10.1021/acsami.0c06672.

[41] M. Sarker, J.Y. Song, S.H. Jhung, Carboxylic-acid-functionalized UiO-66-NH_2: A promising adsorbent for both aqueous- and non-aqueous-phase adsorptions, J. Chem. Eng. 331 (2018) 124-131.

[42] C. Du, B. Zhao, X.-B. Chen, N. Birbilis, H. Yang, Effect of water presence on choline chloride-2urea ionic liquid and coating platings from the hydrated ionic liquid, Sci. Rep. 6 (2016) 29225.

[43] K. Chakarova, I. Strauss, M. Mihaylov, N. Drenchev, K. Hadjiivanov, Evolution of acid and basic sites in UiO-66 and UiO-66-NH2 metal-organic frameworks: FTIR study by probe molecules, Micropor. Mesopor. Mat. 281 (2019) 110-122.

[44] I. Strauss, K. Chakarova, A. Mundstock, M. Mihaylov, K. Hadjiivanov, N. Guschanski, J. Caro, UiO-66 and UiO-66-NH2 based sensors: Dielectric and FTIR investigations on the effect of CO2 adsorption, Micropor. Mesopor. Mat. 302 (2020) 110227.

[45] K.L. Timofeev, S.A. Kulinich, T.S. Kharlamova, NH2-modified UiO-66: structural characteristics and functional properties, Molecules. 28 (2023) 3916.

[46] O. Ozalp, Z.P. Gumus, M. Soylak, Metal-organic framework functionalized with deep eutectic solvent for solid-phase extraction of Rhodamine 6G in water and cosmetic products, J Sep Sci. (2023) e2300190.10.1002/jssc.202300190.

[47] O. Ozalp, Z.P. Gumus, M. Soylak, MIL-101 (Cr) metal–organic frameworks based on deep eutectic solvent (ChCl: Urea) for solid phase extraction of imidacloprid in tea infusions and water samples, J. Mol. Liq. 378 (2023) 121589.

[48] P. Makoś, E. Słupek, J. Gębicki, Extractive detoxification of feedstocks for the production of biofuels using new hydrophobic deep eutectic solvents–Experimental and theoretical studies, J. Mol. Liq. 308 (2020) 113101.

[49] P. Makoś-Chełstowska, M. Kaykhaii, J. Płotka-Wasylka, M. de la Guardia, Magnetic deep eutectic solvents–Fundamentals and applications, J. Mol. Liq. 365 (2022) 120158.

Caption of tables

Table 1

Optimal values of process parameters for selective and universal removal of HMF, FF, HQ and VAN in the range of experiment.

Table 2

The parameters of the real samples subjected to universal and selective removal of HMF, FF, HQ and VAN.

Table S1

FF, HMF, HQ and VAN removal parameters and their corresponding levels in BBD.

Table S2

BBD data matrix: the model-predicted and experimental RE of FF, HMF, HQ, VAN from model samples.

Table S3

Analysis of variance (ANOVA) for BBD with respect to selective and universal removal of HMF, FF, HQ, VAN.

Table S4

Comparison of the ChCl@NH2-UiO-66 method with other literature-reported techniques for removing inhibitory compounds from hydrolysates.

Optimized parameter	X1	X2	X3	X4	R^2	R_{pred}^2	R_{adj}^2
Y HMF	7.63	4.56	8.54	5.69	0.81	0.80	0.74
Y FF	5.15	7.54	8.54	7.16	0.84	0.81	0.78
Y HQ	5.74	8.02	1.98	7.94	0.79	0.74	0.71
Y VAN	5.15	4.12	1.87	7.82	0.93	0.84	0.82
Y	11.16	5.86	8.77	4.97	0.79	0.71	0.68

Sample code	Sample origin	Initial concentrations (mgL^{-1})	RE (%) of selected substance for selective and universal (Y) removal according to optimized process parameters				
			Y HMF	Y FF	Y HQ	Y VAN	Y
1.1	hardwood blend after pre-treatment with 5% H_2SO_4	HQ 7.02 HMF 2.10 FF 1.05 VAN 2.34	62.21±0.18	48.33±0.48	38.21±0.34	54.26±0.77	44.58±0.36
1.2	hardwood blend after pre-treatment with 30% H_2SO_4	HQ 29.97 HMF 1.22 FF <LOD VAN 1.92	61.47±0.45	<LOD	37.51±0.29	53.78±0.91	42.15±0.69

1.3	hardwood blend after pre-treatment with 0.5M NaOH	HQ 27.49 HMF 3.70 FF 1.67 VAN <LOD	58.47±0.38	47.11±0.87	36.22±0.83	<LOD	38.23±0.36
1.4	hardwood blend after pre-treatment with 1.5M NaOH	HQ 42.36 HMF 2.47 FF 2.15 VAN 2.39	64.24±0.28	49.01±0.28	38.54±0.44	51.98±0.14	37.59±0.98
1.5	hardwood blend after pre-treatment with 5% H_2O_2	HQ <LOD HMF 31.71 FF <LOD VAN <LOD	62.17±0.95	<LOD	<LOD	<LOD	61.58±0.32
1.6	hardwood blend after	HQ <LOD HMF 41.60	61.33±0.35	<LOD	<LOD	55.21±0.84	60.38±0.85

	pre-treatment with 30% H_2O_2	FF <LOD VAN 2.09					
1.7	starch and lignocellulose hydrolyzate from potato processing. after centrifugation (industrial by-product)	HQ 14.60 HMF 4.62 FF 3.50 VAN 4.89	57.36±0.88	45.74±0.26	35.47±0.73	54.78±0.35	39.52±0.65
1.8	starch and lignocellulose hydrolyzate from potato	HQ 40.69 HMF 3.20 FF 1.58 VAN 1.86	57.87±0.92	48.26±0.31	39.54±0.68	55.13±0.48	41.58±0.49

	processing additionally pre-treated with 5%H2SO4							
1.9	starch and lignocellulose hydrolyzate from potato processing additionally pre-treated with 0.5 M NaOH	HQ 16.46 HMF 3.28 FF 2.17 VAN 6.91	59.38±0.17	47.68±0.75	34.59±0.59	53.62±0.83	36.59±0.47	
2.1	Lignocellulosic biomass	HQ <LOD HMF <LOD	<LOD	46.59±0.65	<LOD	52.99±0.62	49.25±0.36	

	(corn cobs acidic hydrolysis (1.1)	FF 2.79 VAN 6.69					
2.2	Lignocellulosic biomass (corn cobs alkaline hydrolyssis)	HQ <LOD HMF 4.16 FF 1.10 VAN 1.86	60.06±0.27	42.69±0.33	<LOD	51.73±0.46	59.57±0.33
2.3	Lignocellulosic biomass (corn cobs alkaline hydrolyssis)	HQ <LOD HMF 9.30 FF 5.13 VAN 5.59	61.96±1.01	51.22±0.98	<LOD	54.66±0.17	59.48±0.35
2.4	Lignocellulosic biomass	HQ <LOD HMF 14.16	62.55±0.39	<LOD	<LOD	53.85±0.64	61.58±0.88

	after oxidative pre-treatment (1.5)	FF <LOD VAN 7.01					
2.5	Lignocellulosic biomass after alkaline pre-treatment (1.3)	HQ <LOD HMF 4.08 FF 2.30 VAN 1.95	53.21±0.27	48.11±0.64	<LOD	54.36±0.29	54.01±0.84

Limit of detection (LOD) for HQ=4.2 μgL^{-1}, HMF=0.54 μgL^{-1}, FF=0.30 μgL^{-1}, and VAN= 2.3 μgL^{-1}; Limit of quantification (LOQ) for HQ=14.0 μgL^{-1}, HMF=1.8 μgL^{-1}, FF=1.0 μgL^{-1} and VAN=7.8 μgL^{-1}.

Figure

Click here to access/download;Figure;Figure_1.tif

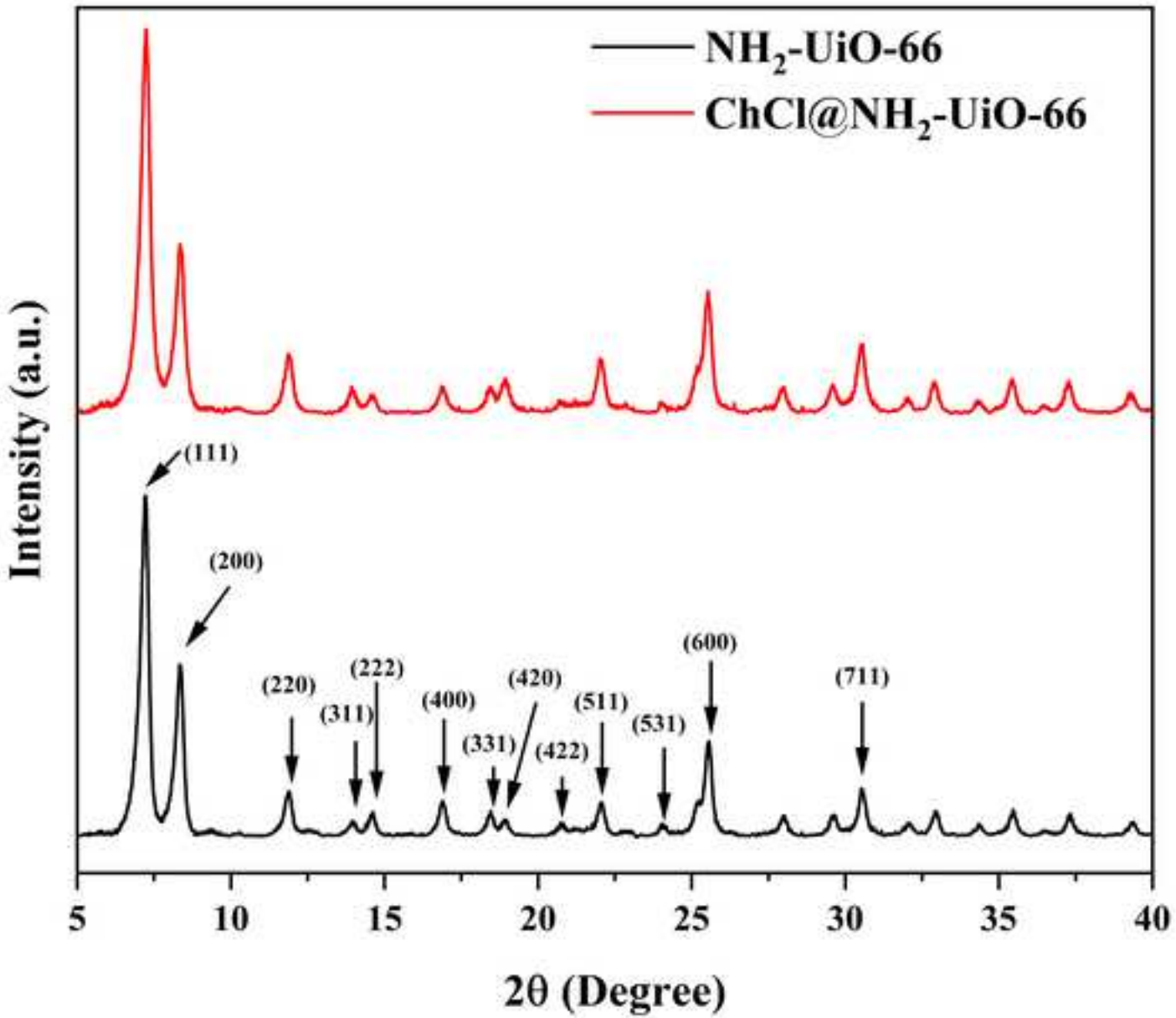

Figure

Click here to access/download;Figure;Figure_2.tif

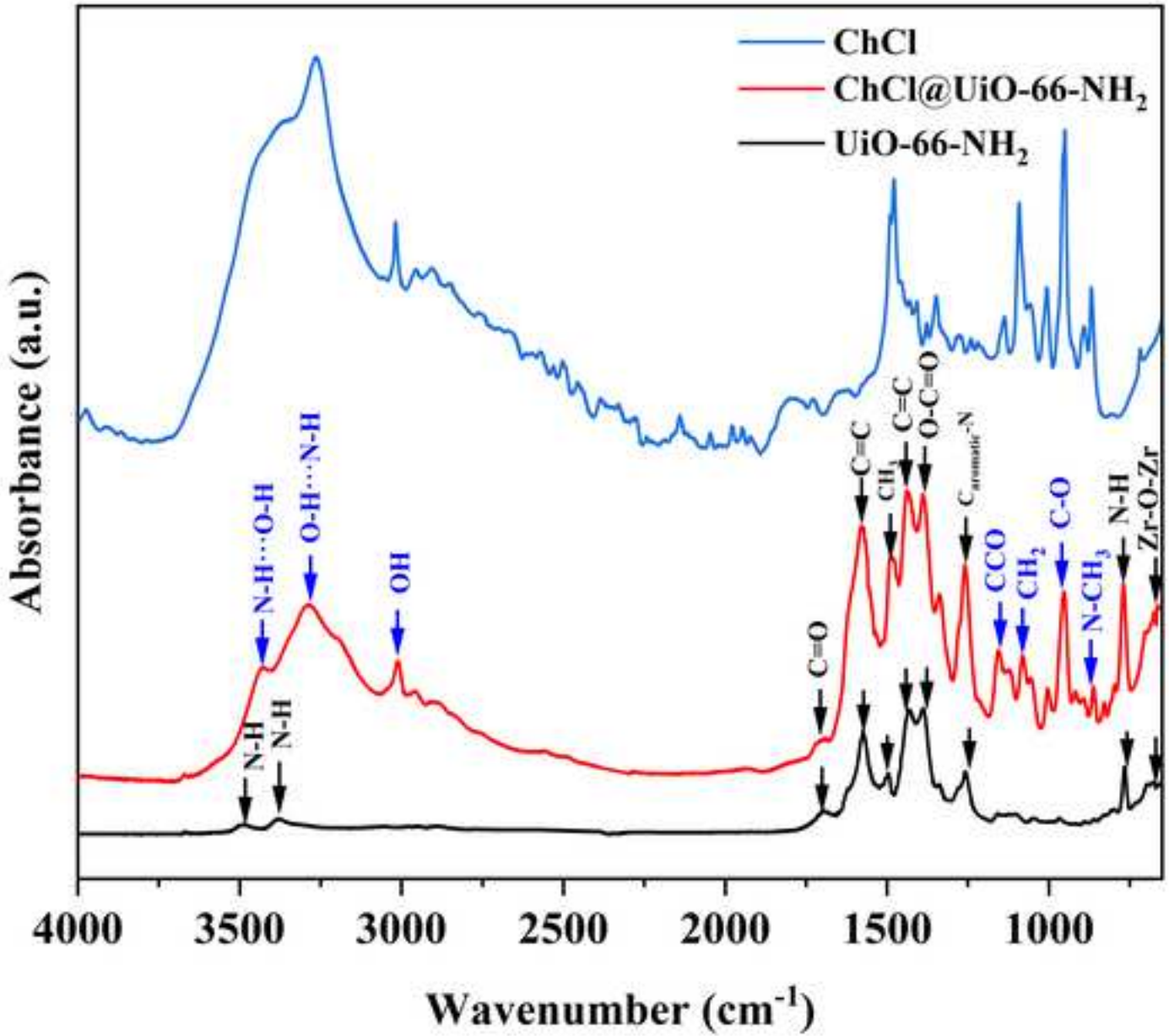

Figure

Click here to access/download;Figure;Figure_3.tif

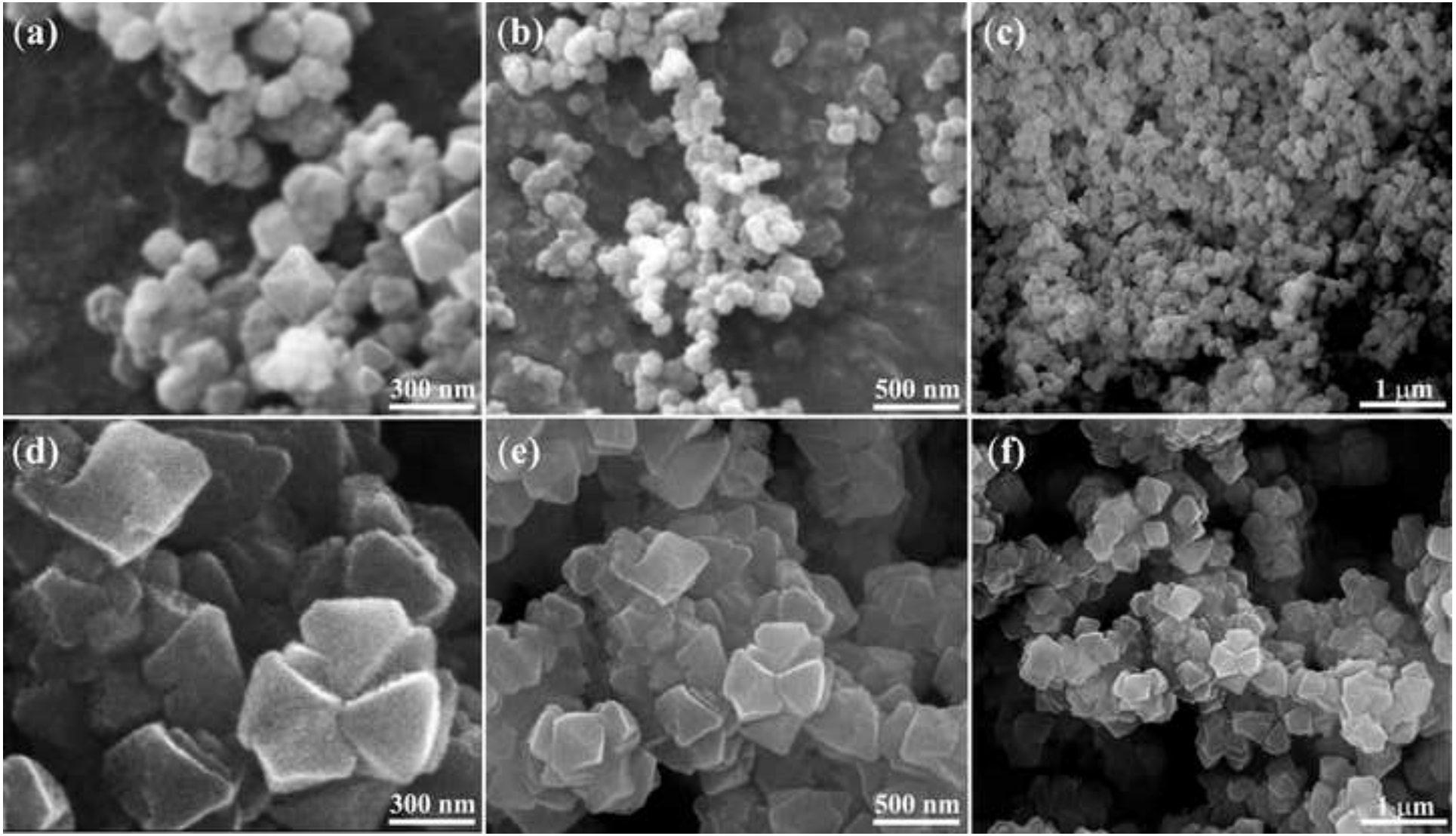

Figure

Click here to access/download;Figure;Figure_4.tif

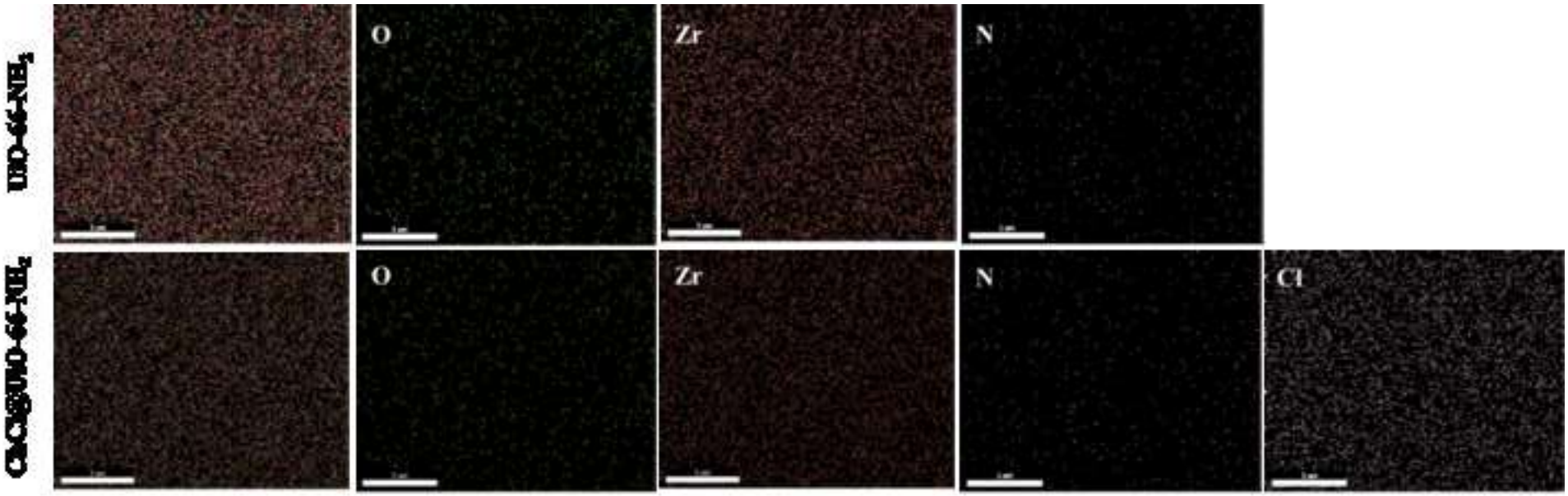

Figure

Click here to access/download;Figure;Figure_5.tif

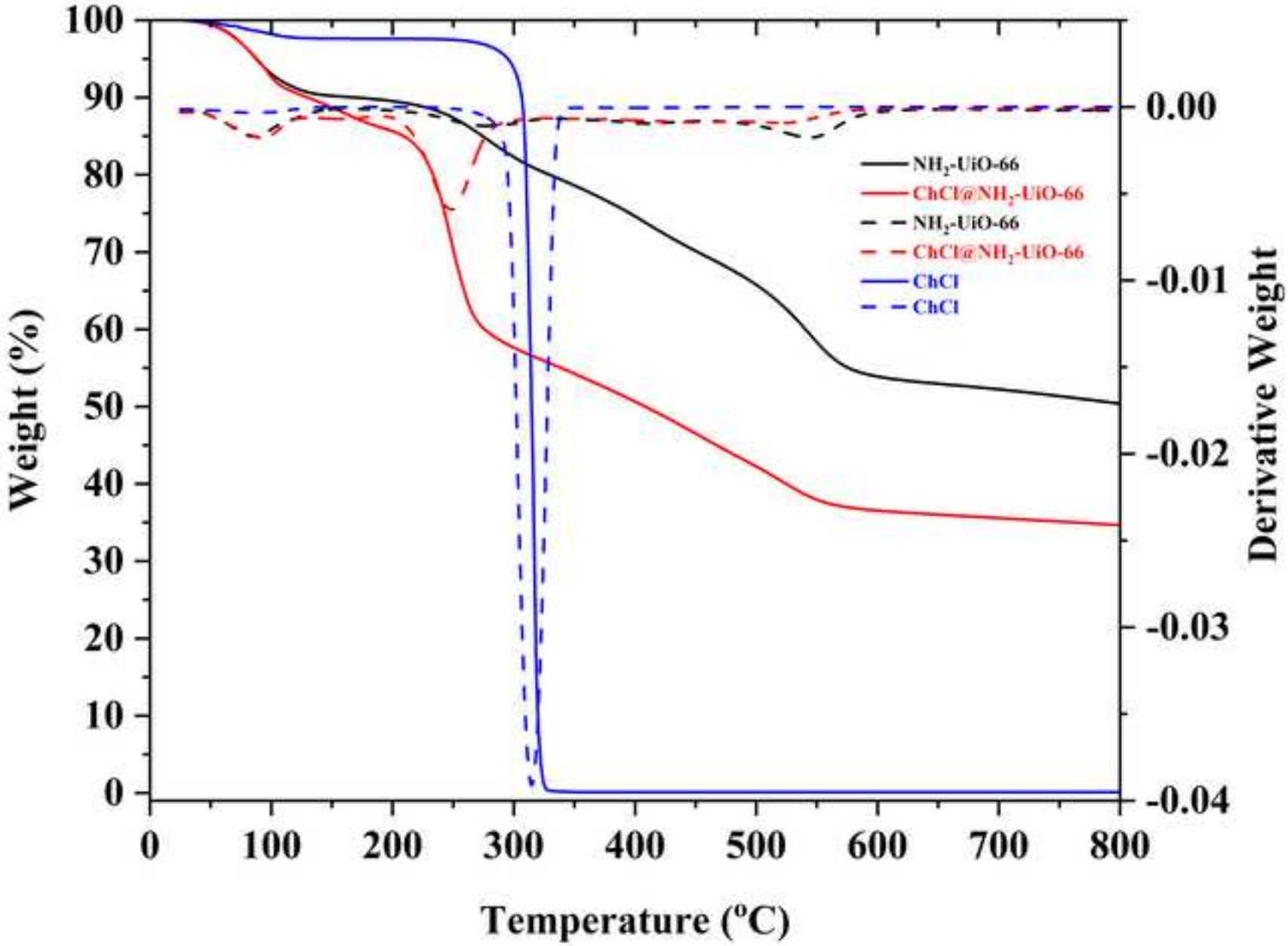

Figure

Click here to access/download;Figure;Figure_6.tif

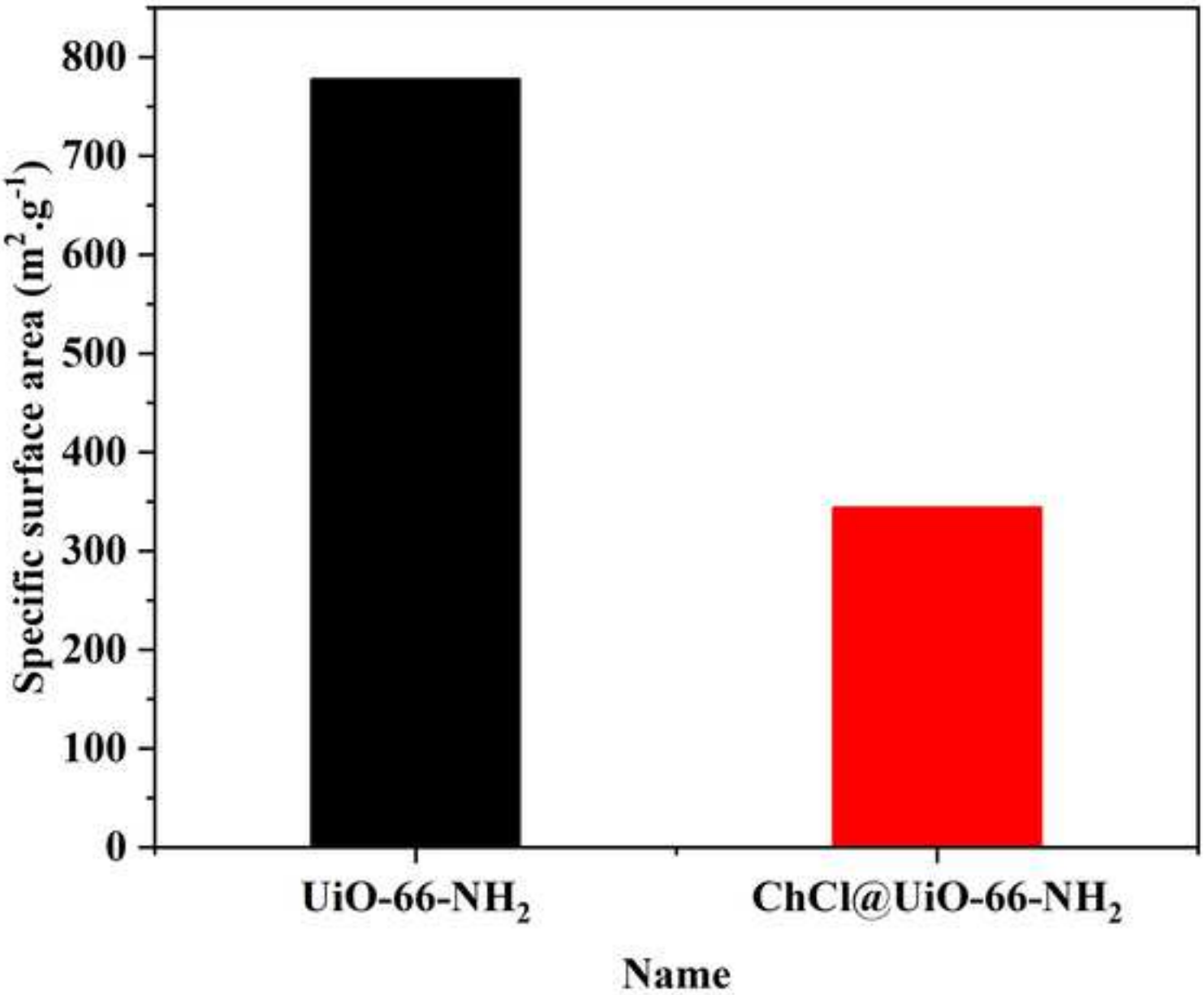

Figure

Click here to access/download;Figure;Figure_7.tif

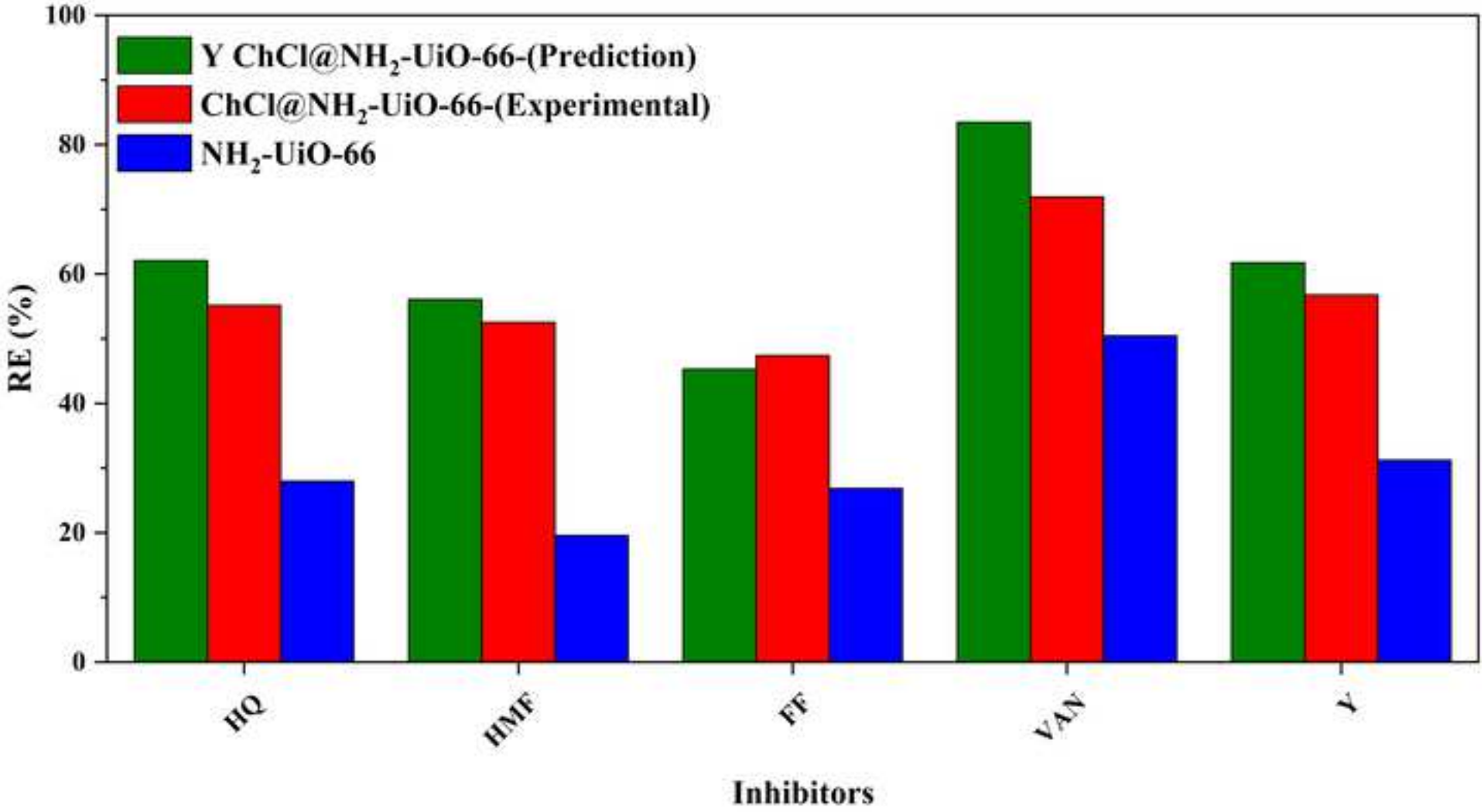

Figure

Click here to access/download;Figure;Figure_8.tif

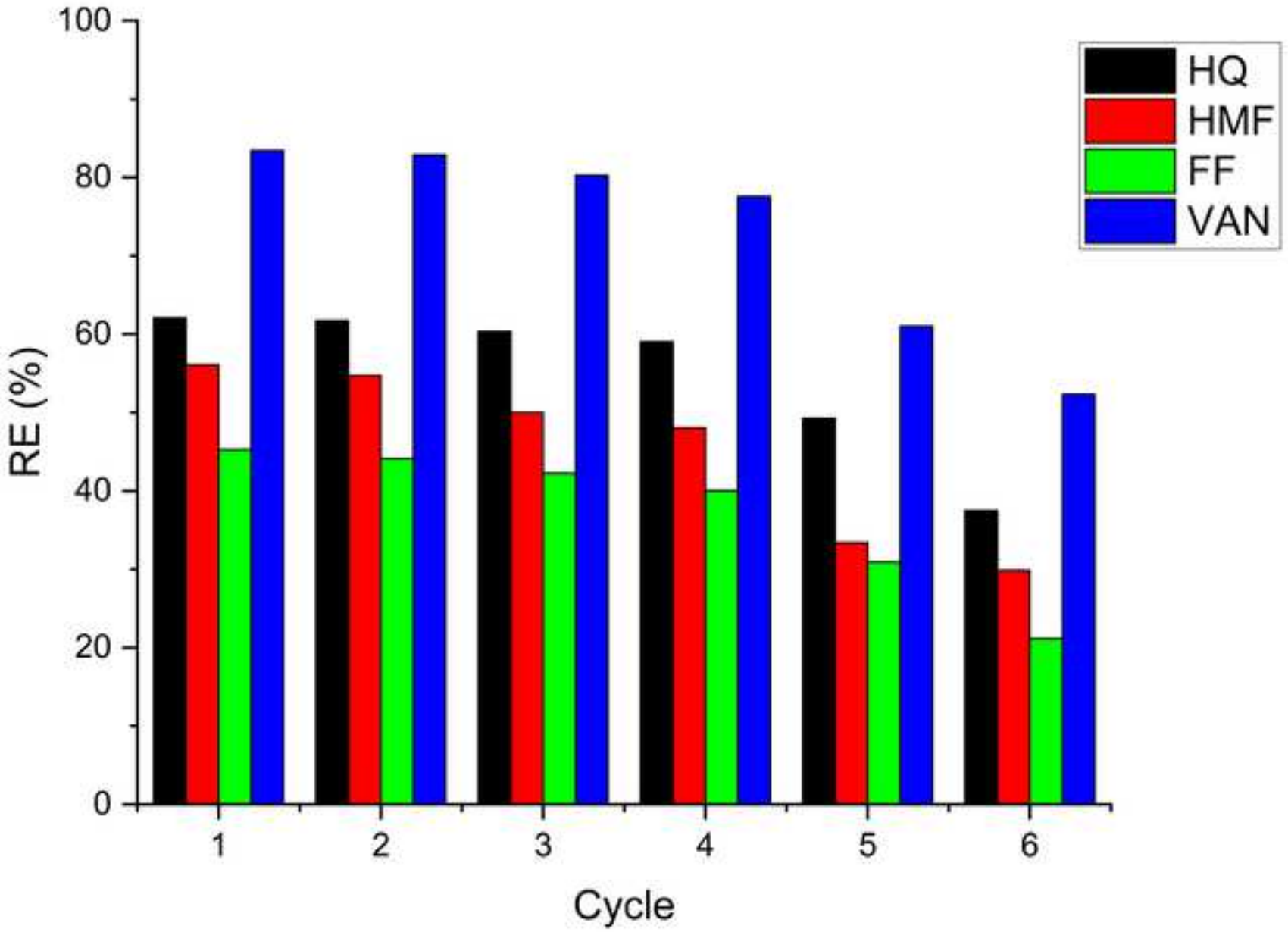

Figure

Click here to access/download;Figure;Figure_S1.png

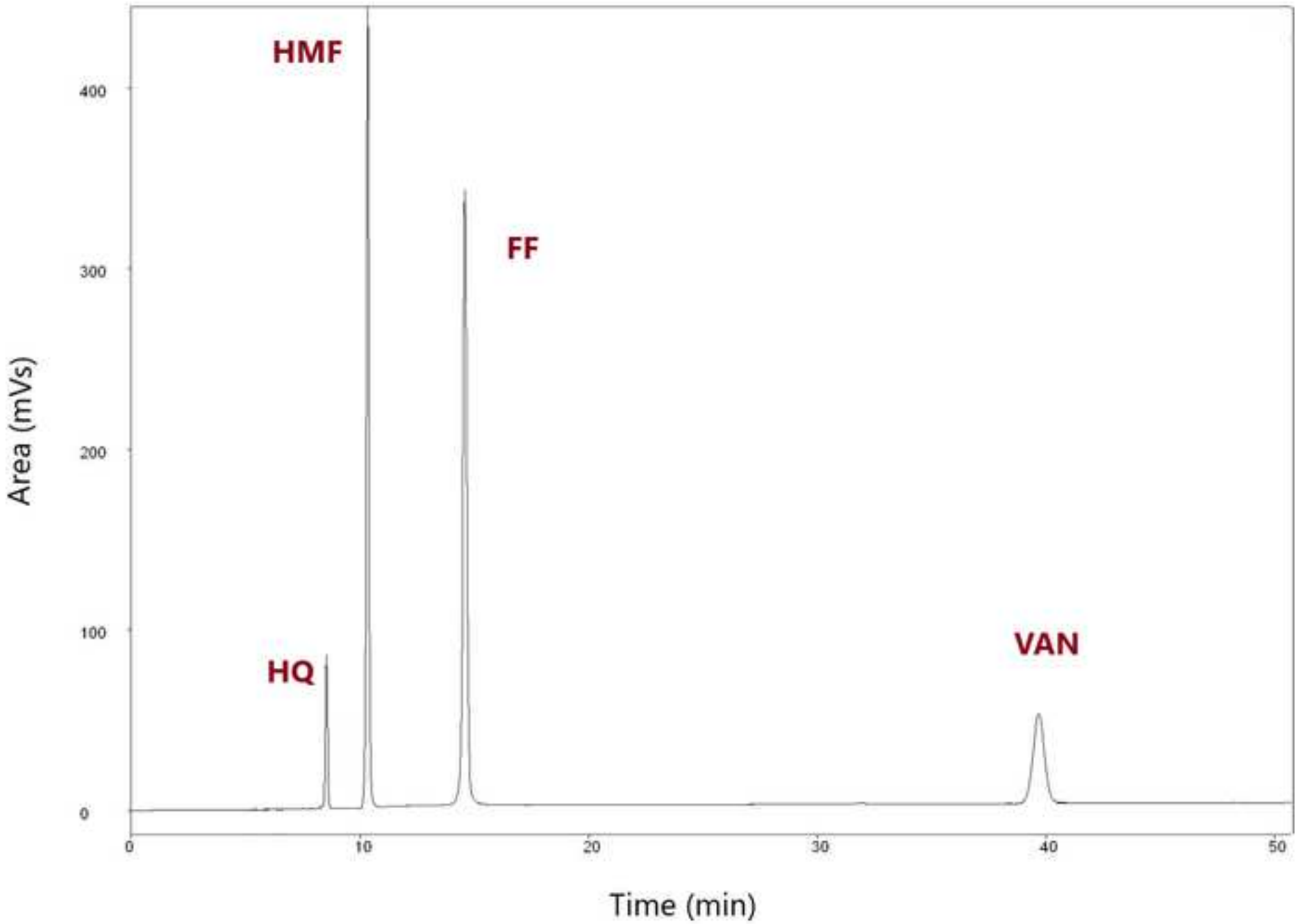

Figure

Click here to access/download;Figure;Figure_S2.png

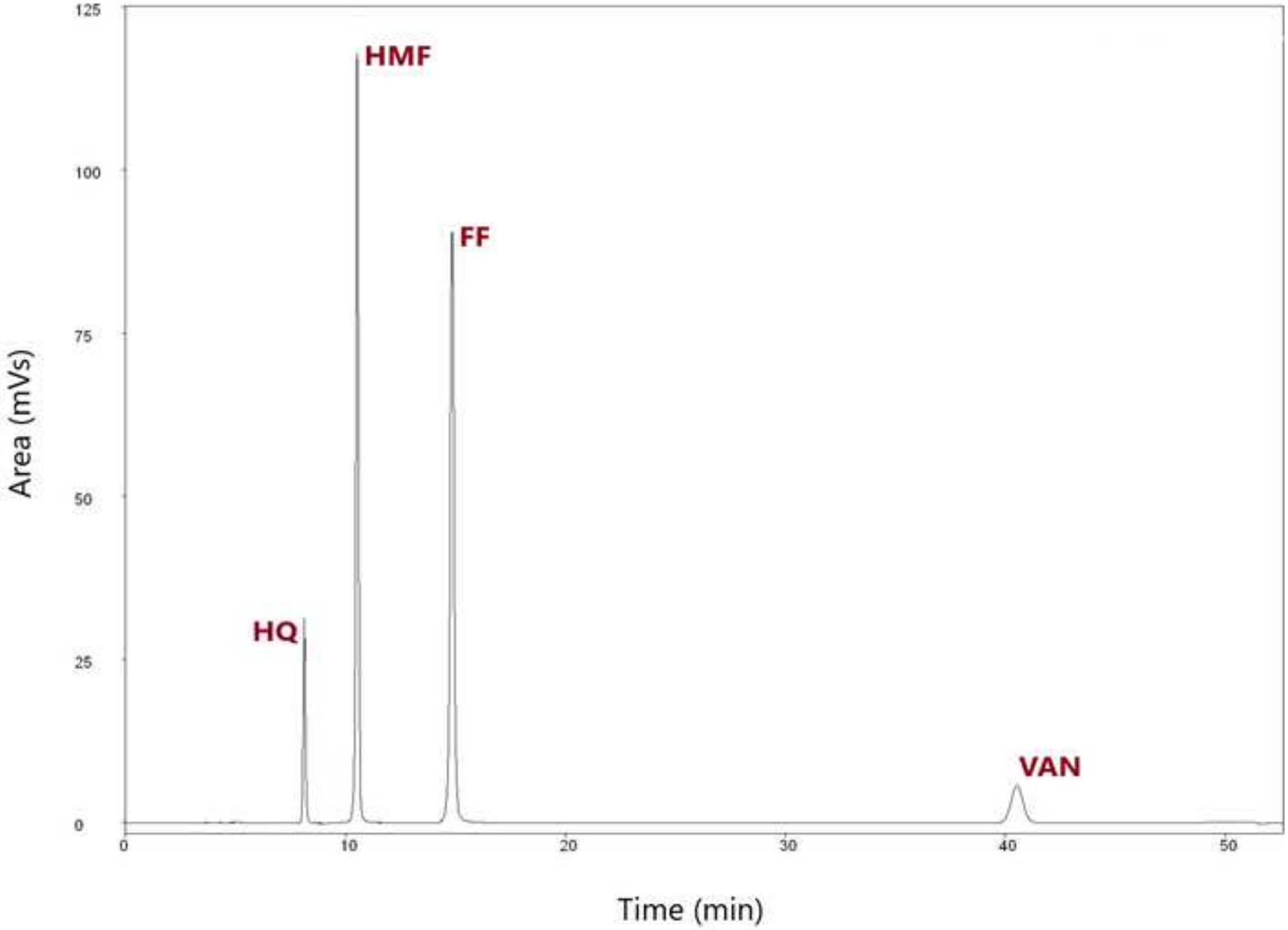

Figure

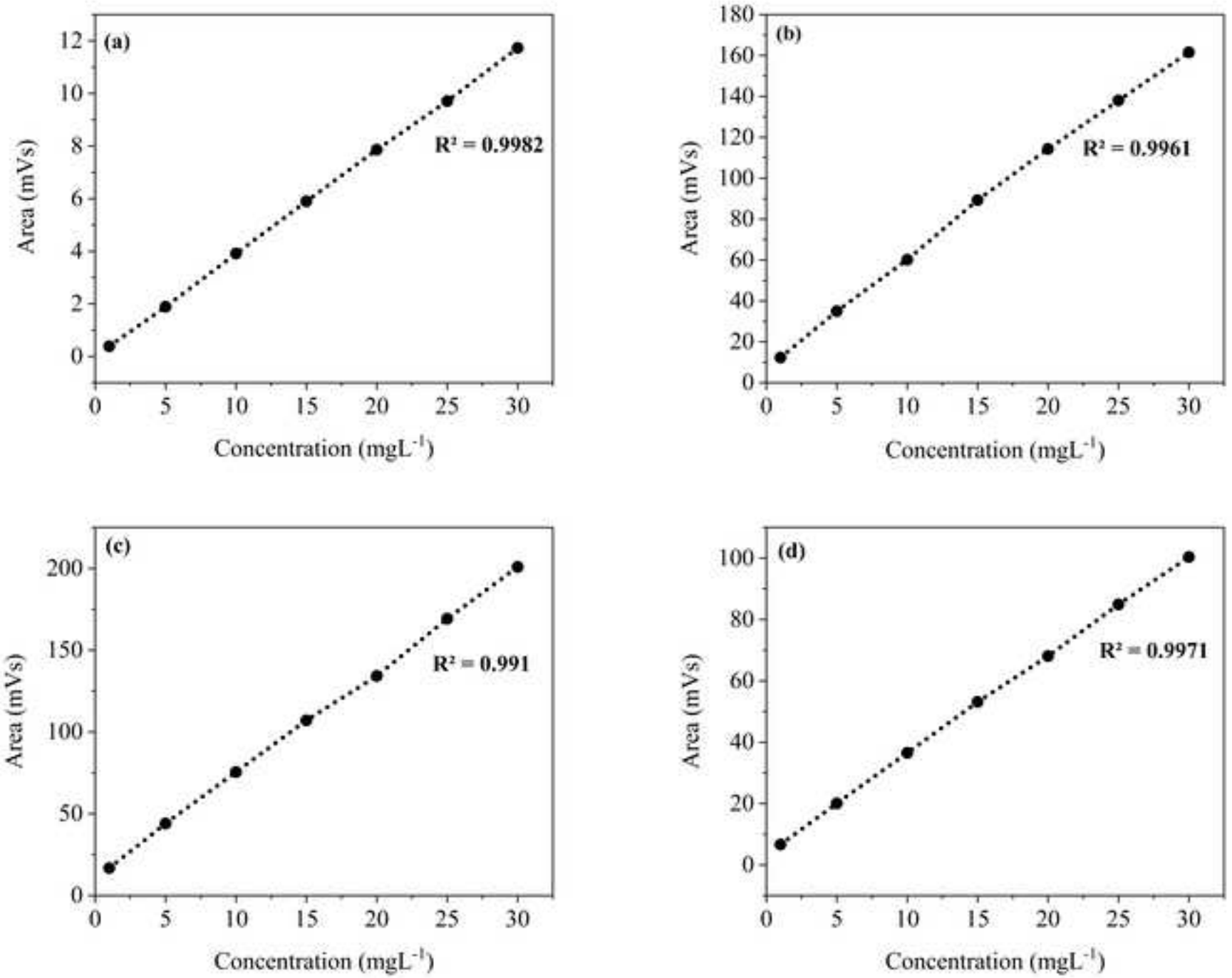

Figure

Click here to access/download;Figure;Figure_S4.tif

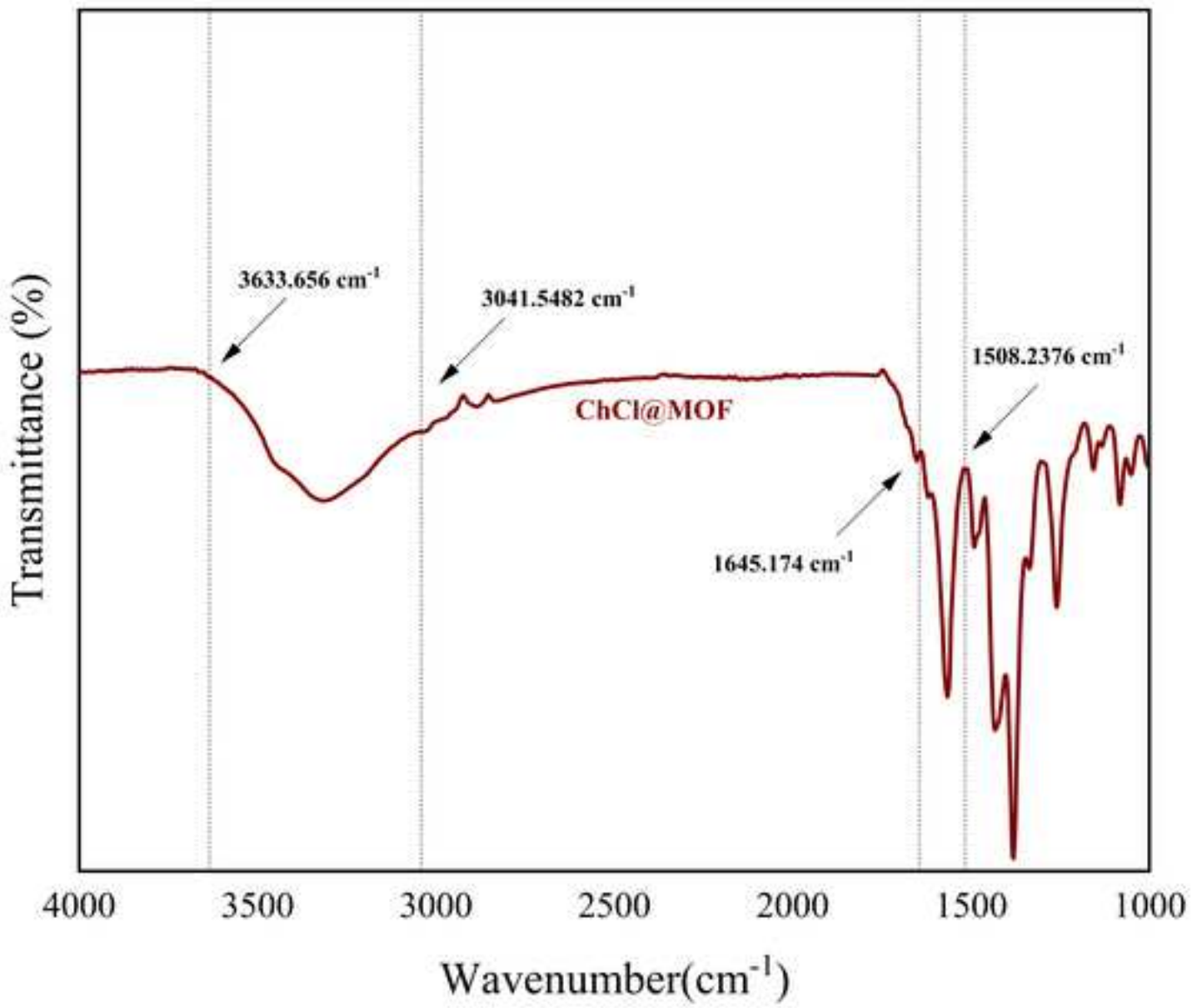

Figure

Click here to access/download;Figure;Figure_S5.tif

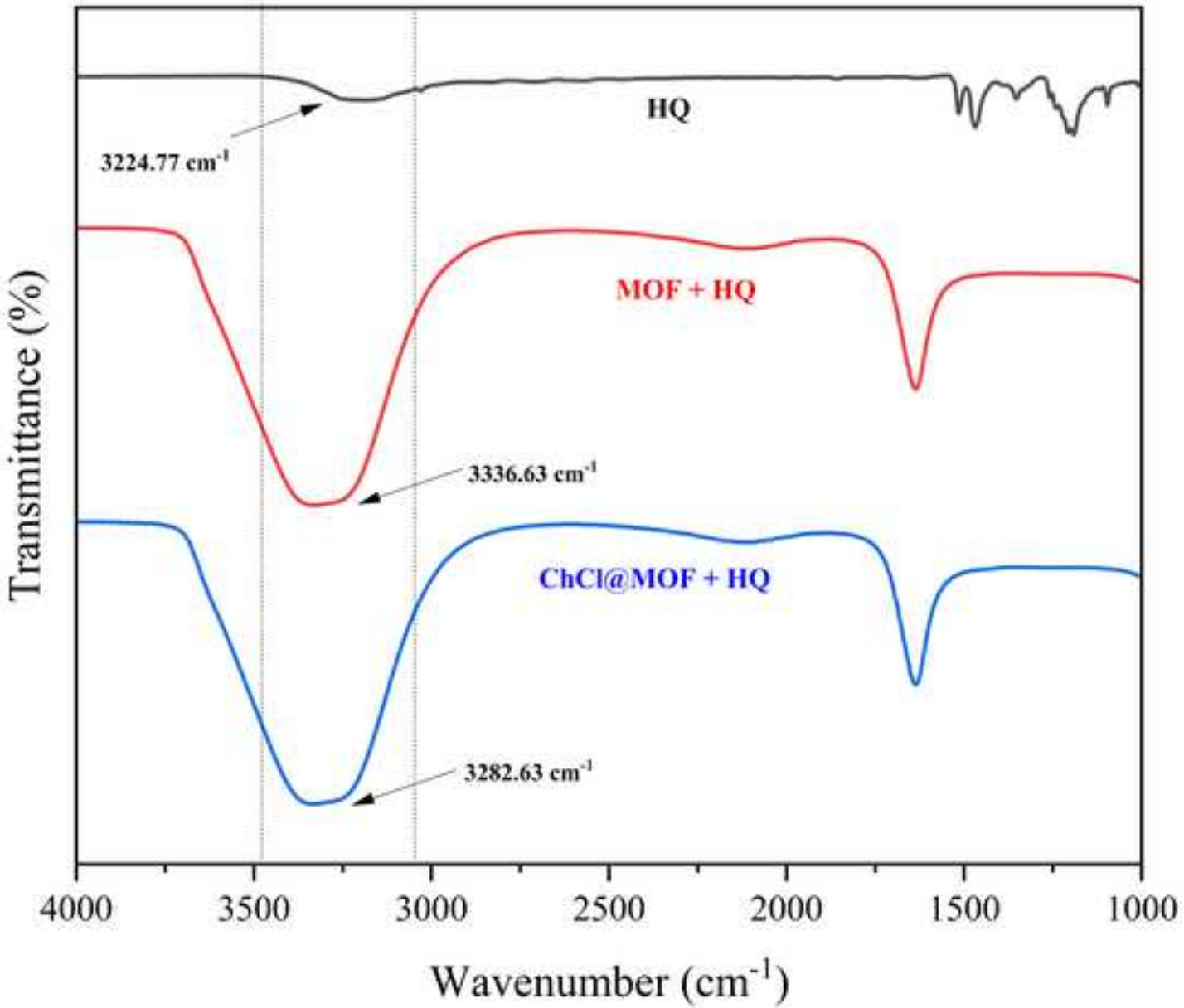

Figure

Click here to access/download;Figure;Figure_S6.tif

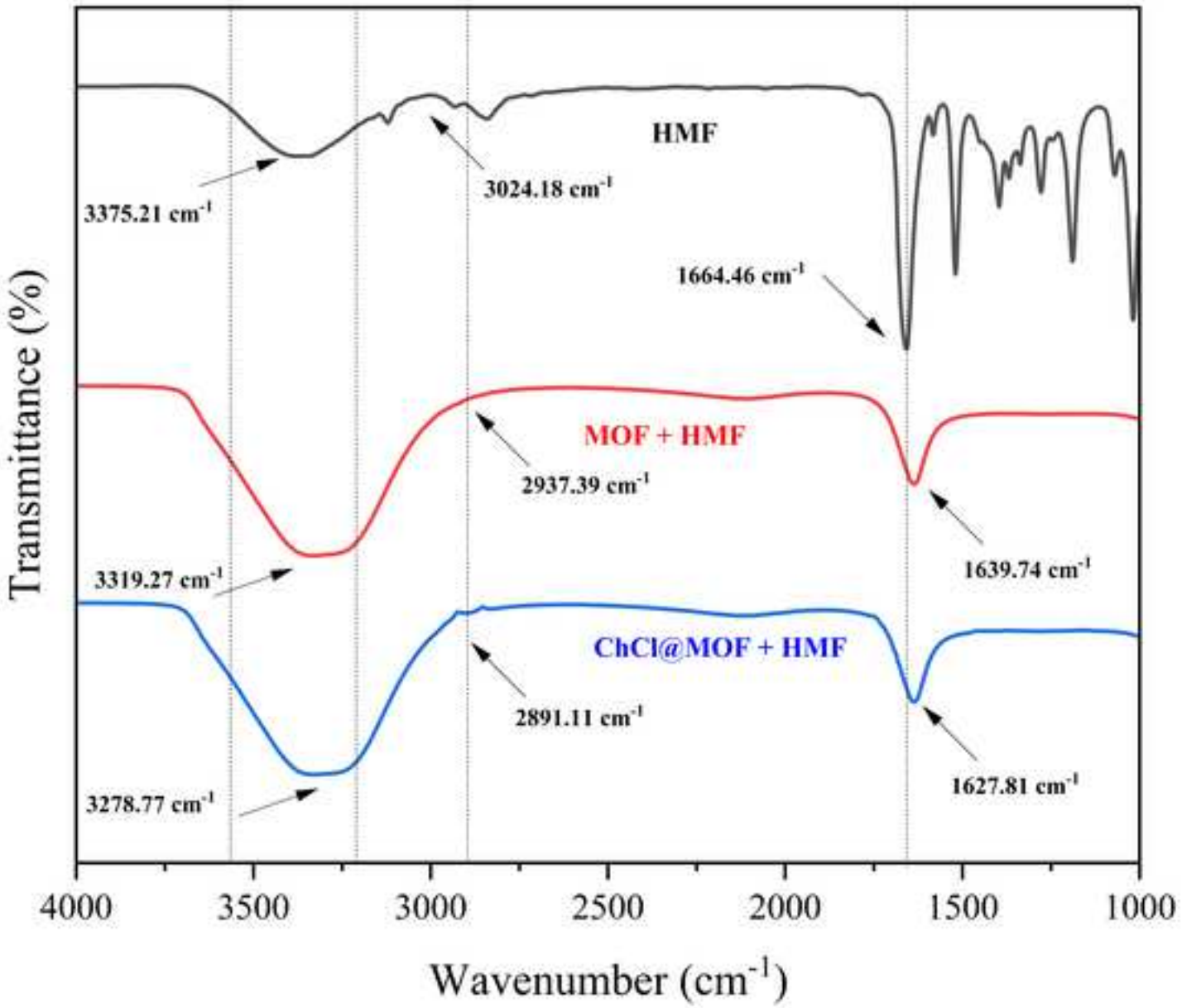

Figure

Click here to access/download;Figure;Figure_S7.tif

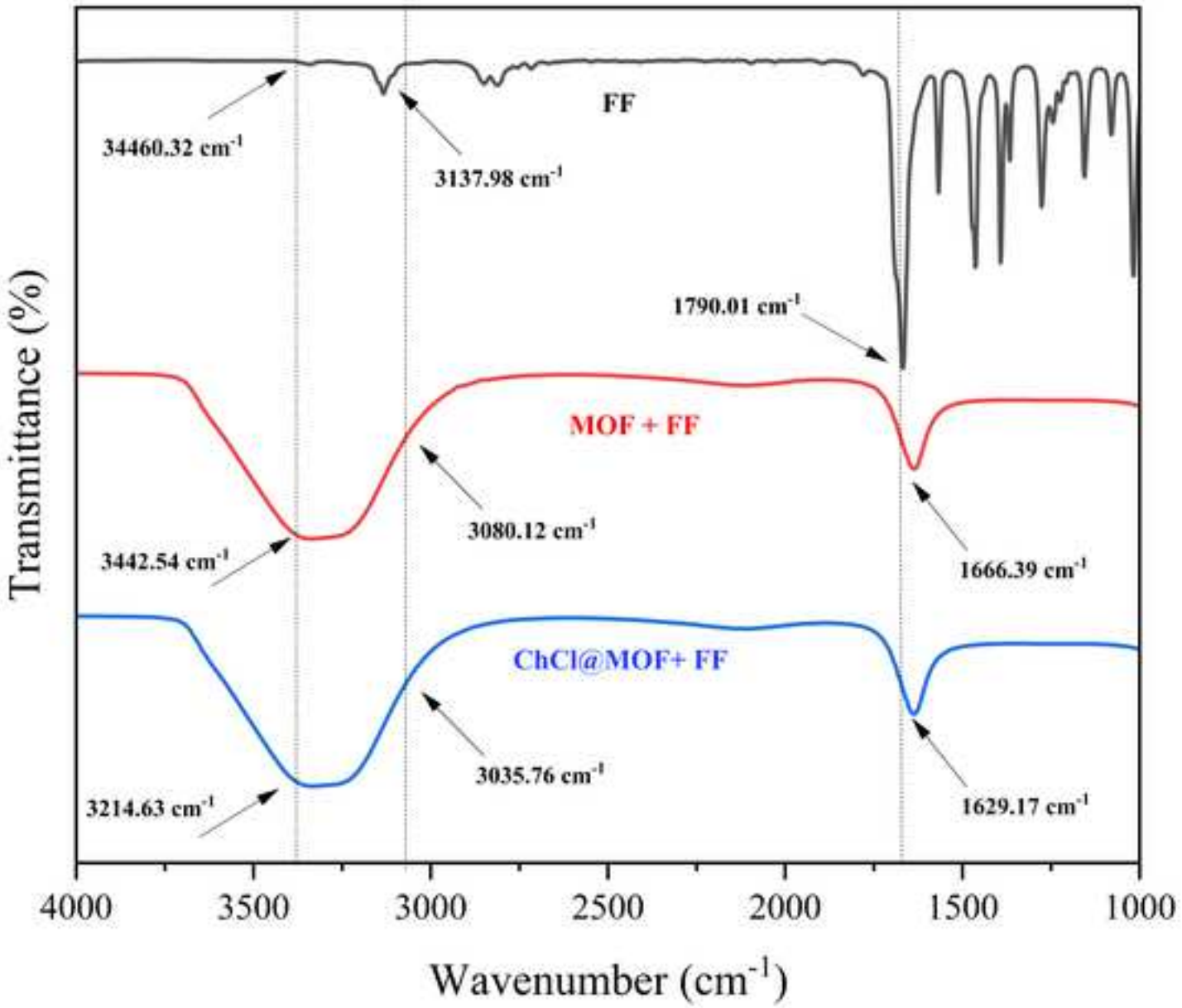

Figure

Click here to access/download;Figure;Figure_S8.tif

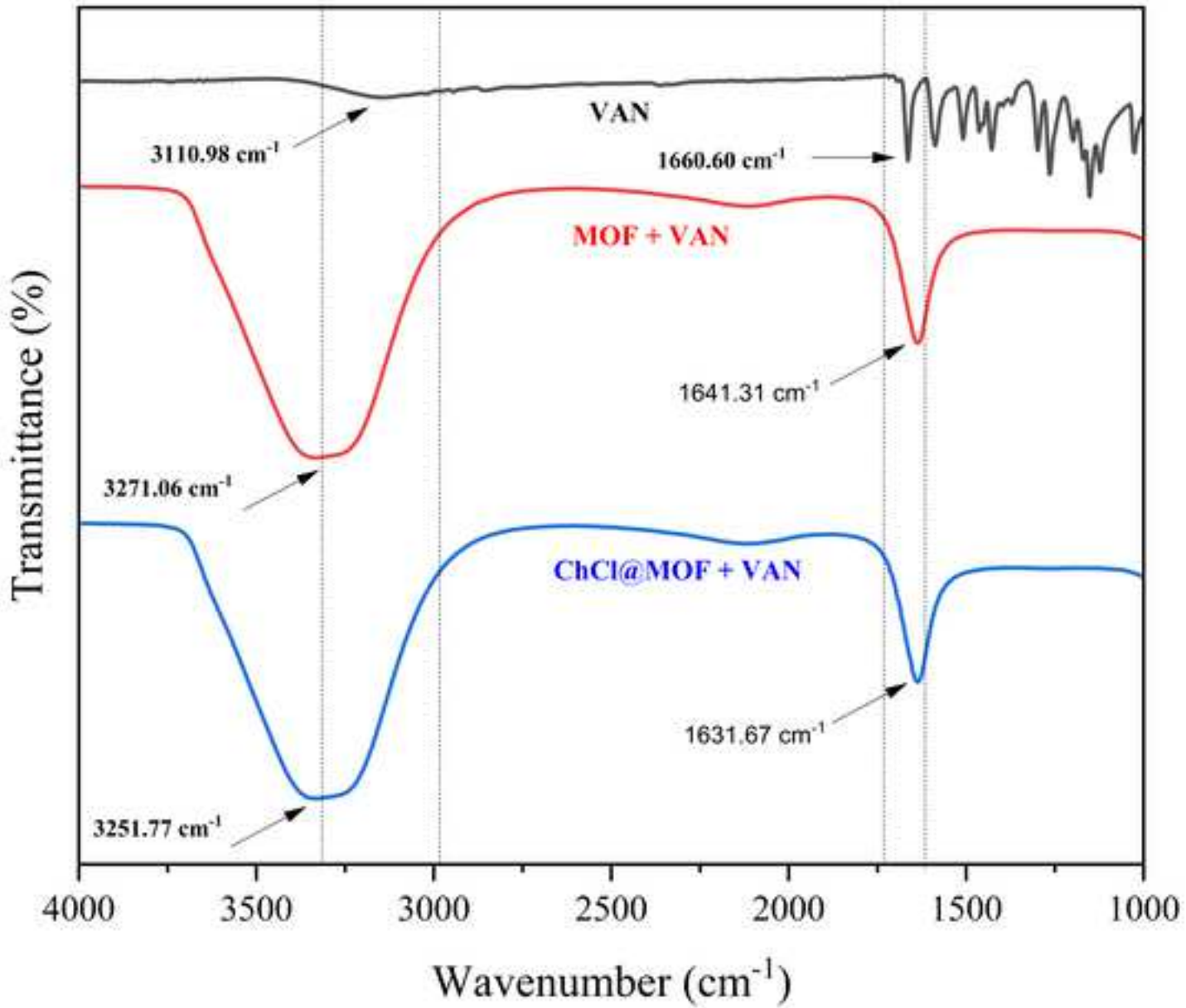

Figure

Click here to access/download;Figure;Figure_S9a.tif

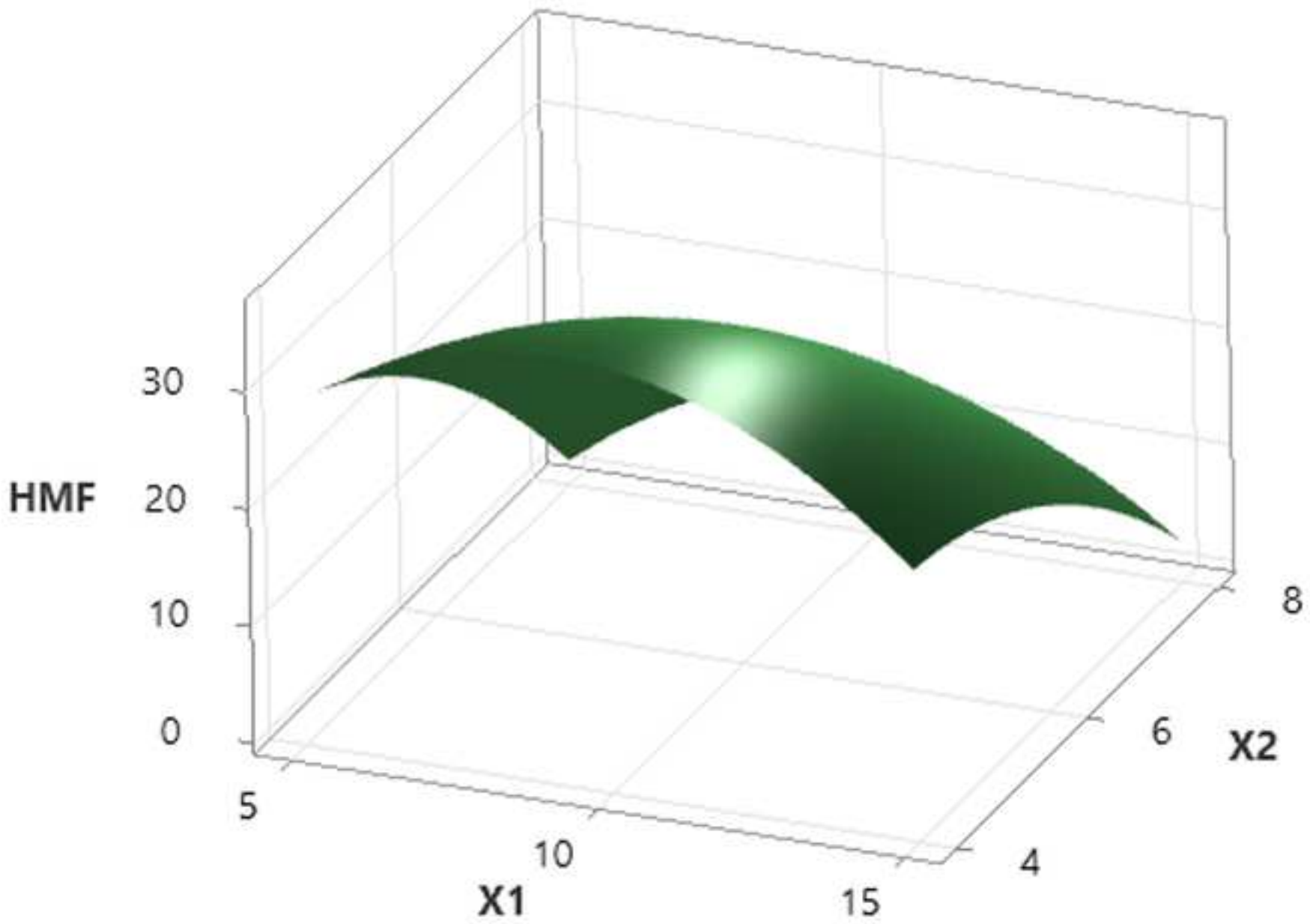

Figure

Click here to access/download;Figure;Figure_S9b.tif

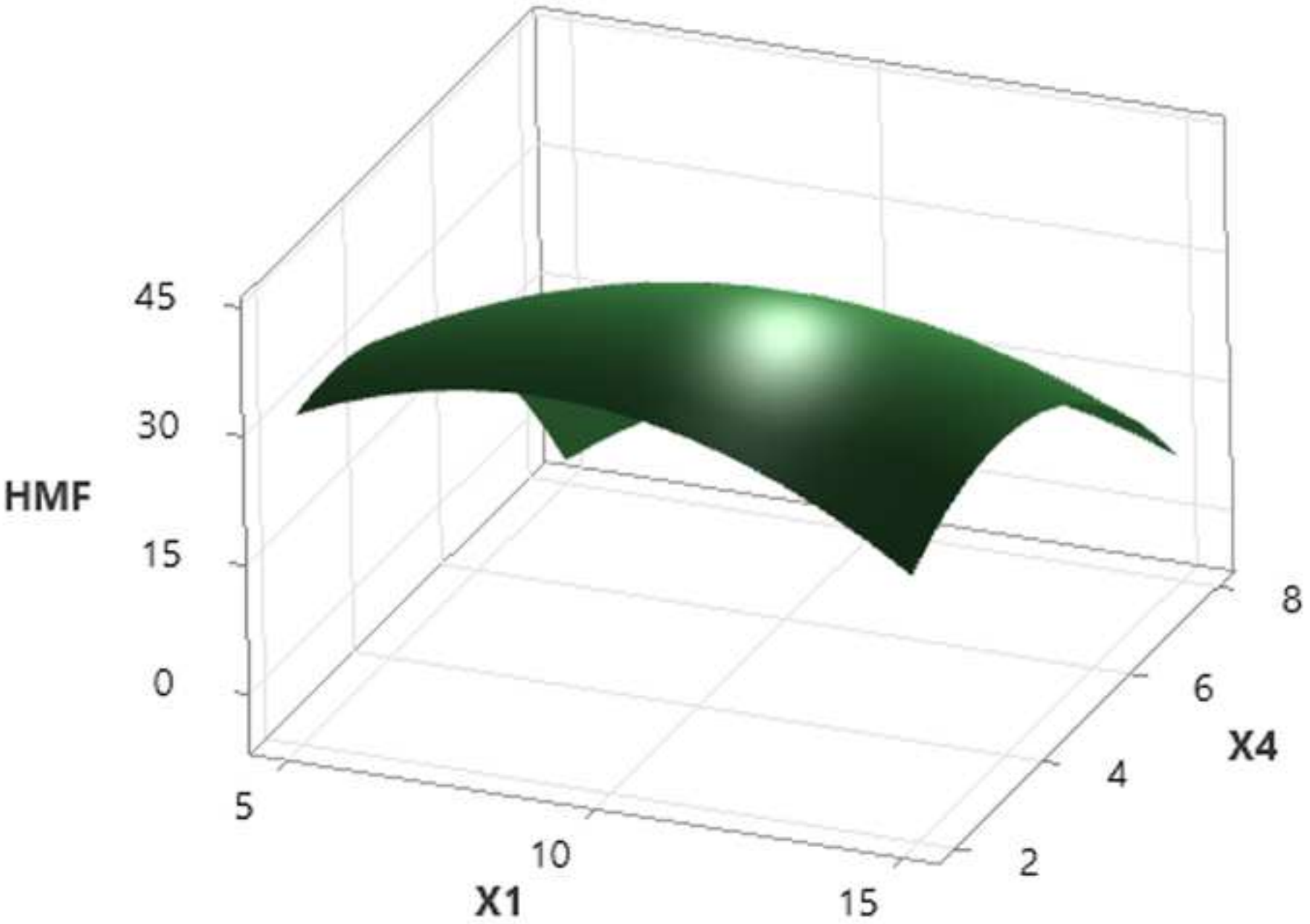

Figure

Click here to access/download;Figure;Figure_S10a.tif

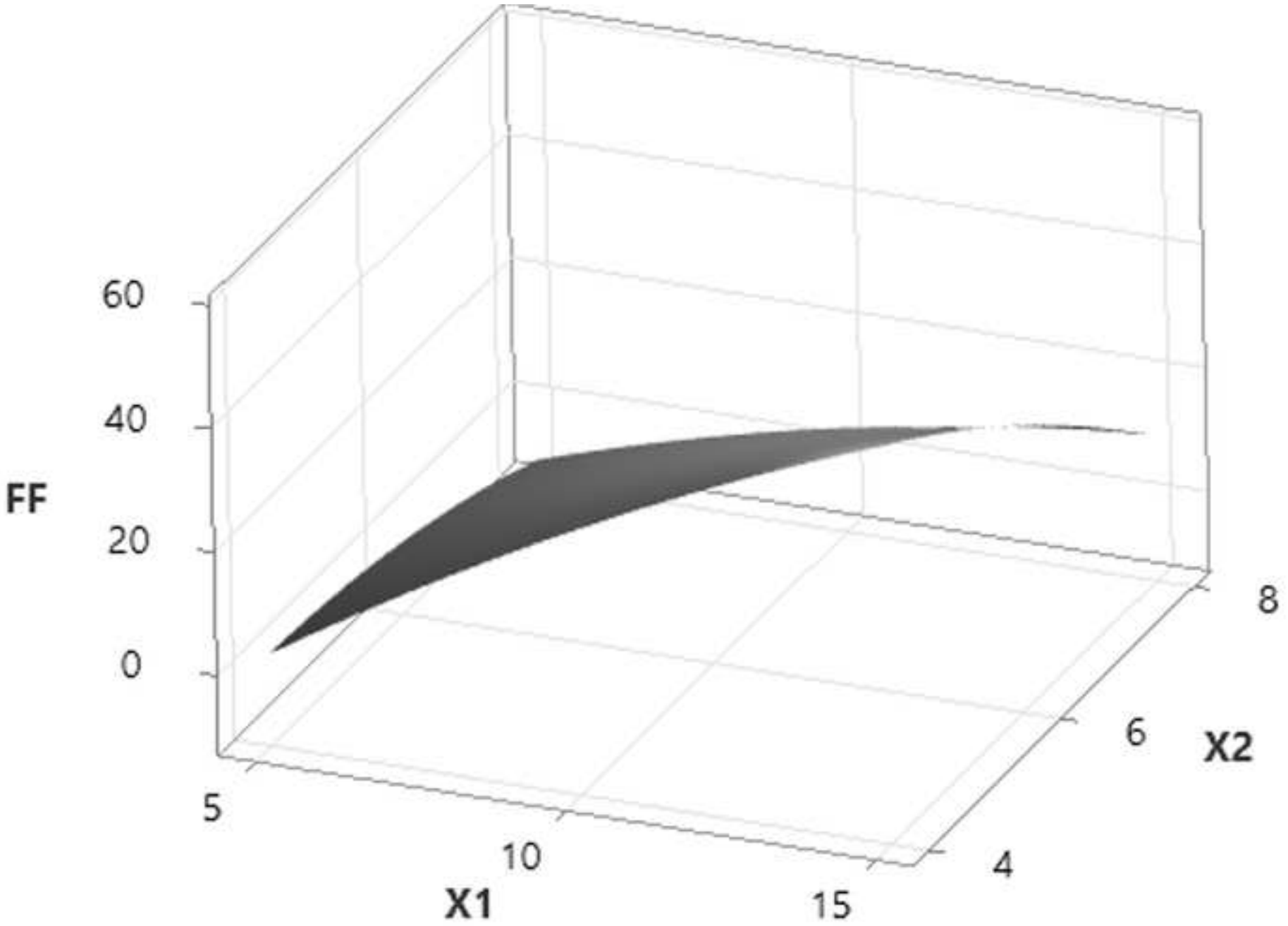

Figure

Click here to access/download;Figure;Figure_S10b.tif

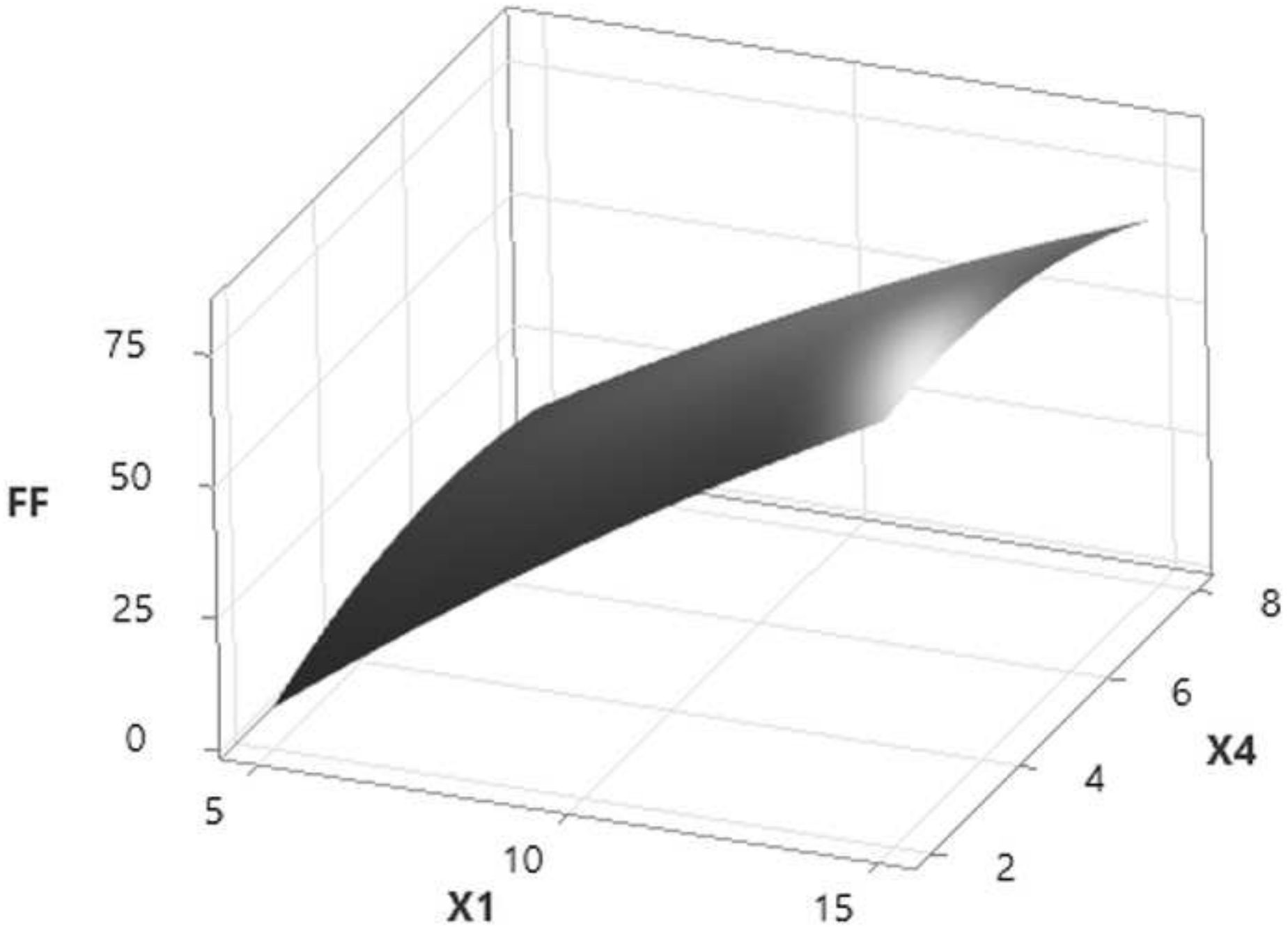

Figure

Click here to access/download;Figure;Figure_S11a.tif

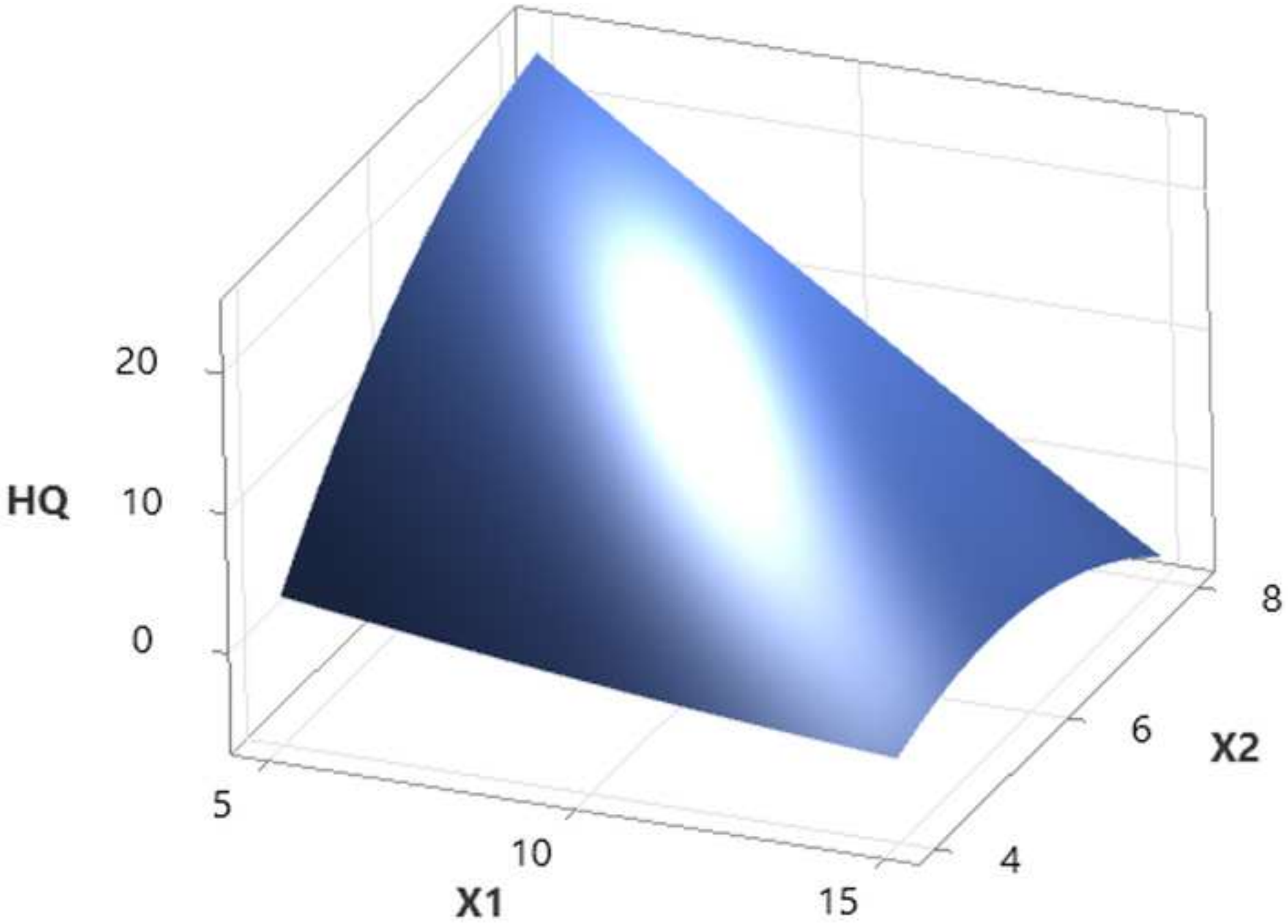

Figure

Click here to access/download;Figure;Figure_S11b.tif

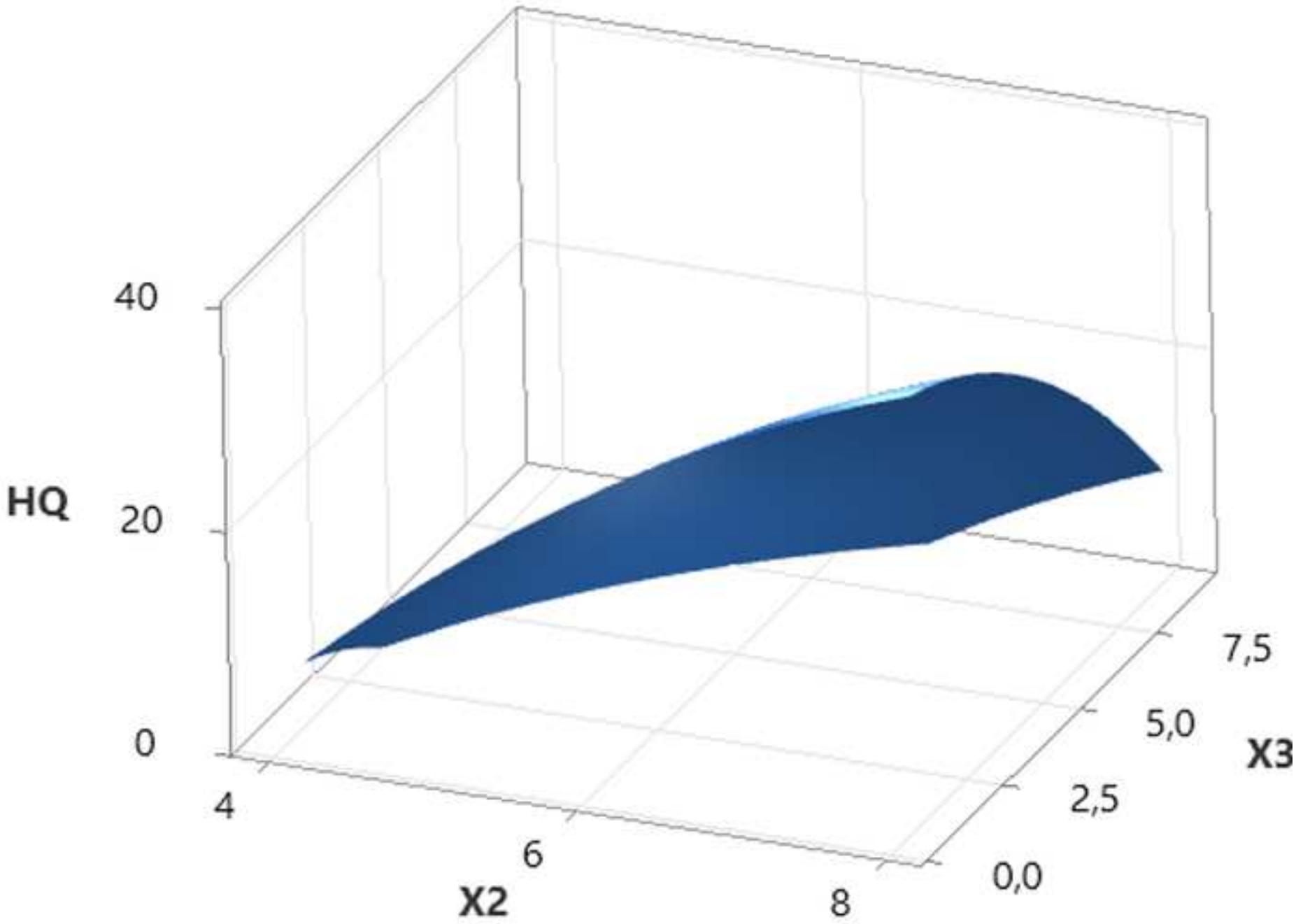

Figure

Click here to access/download;Figure;Figure_S11c.tif

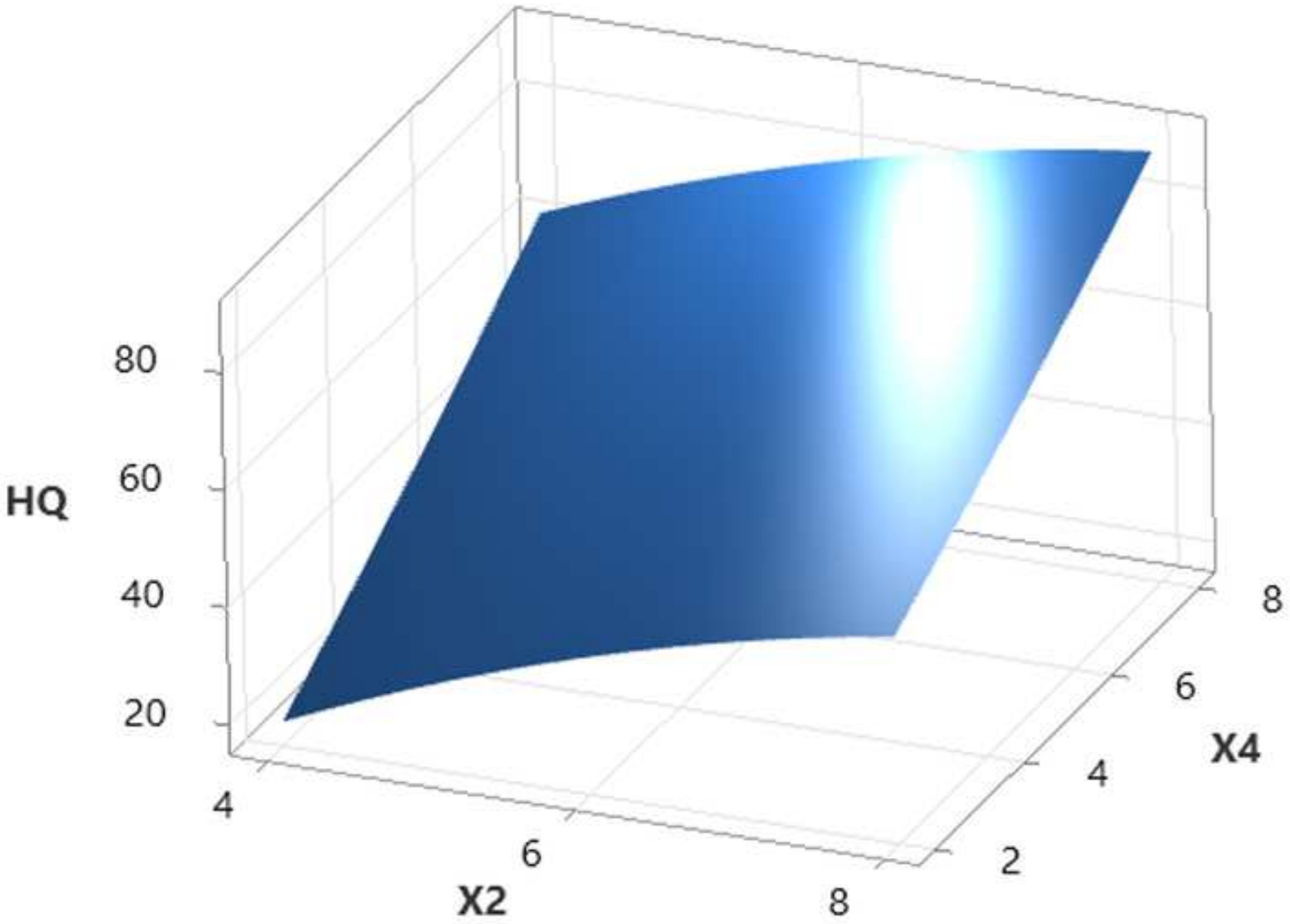

Figure

Click here to access/download;Figure;Figure_S12.tif

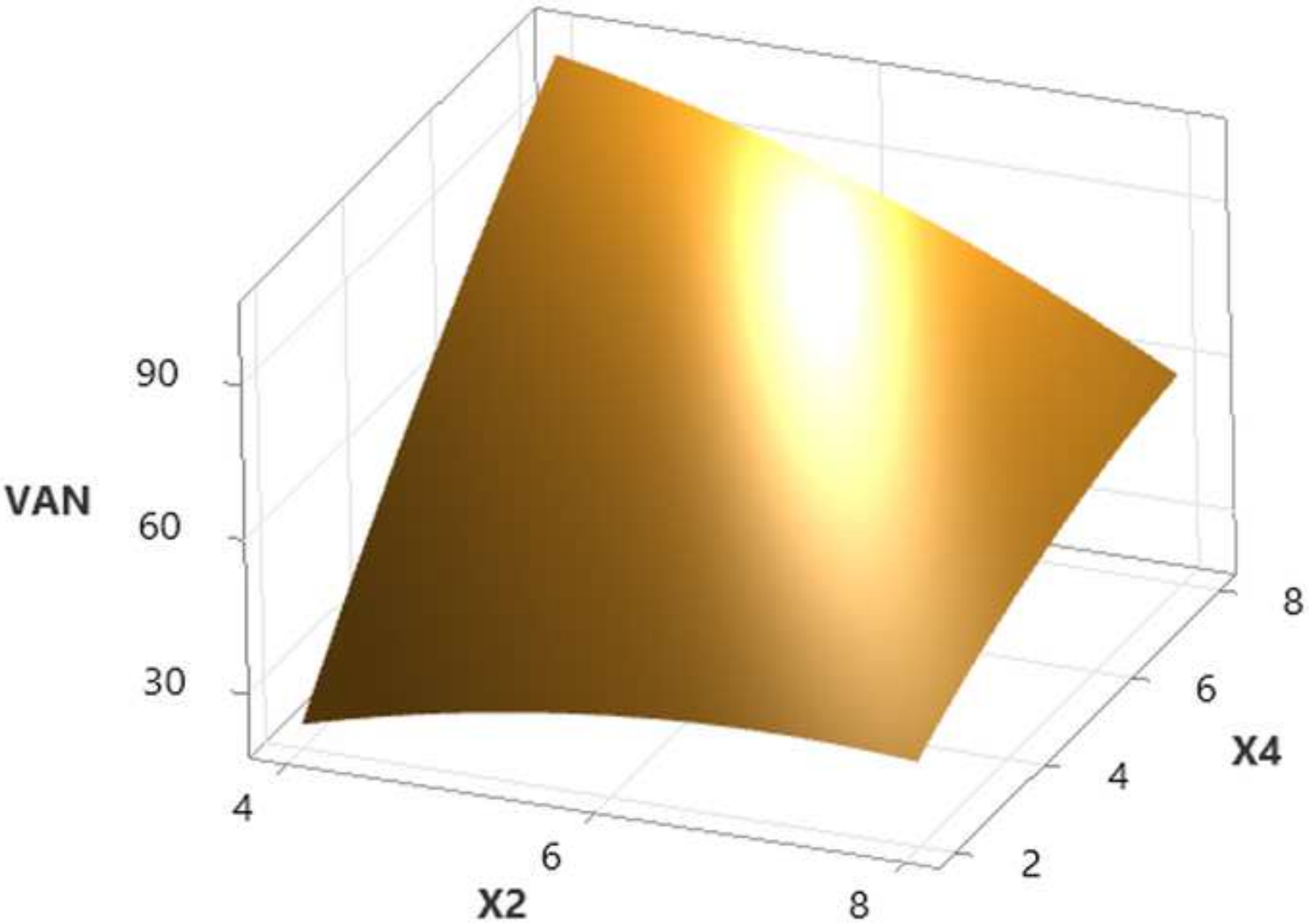

Figure

Click here to access/download;Figure;Figure_S13a.tif

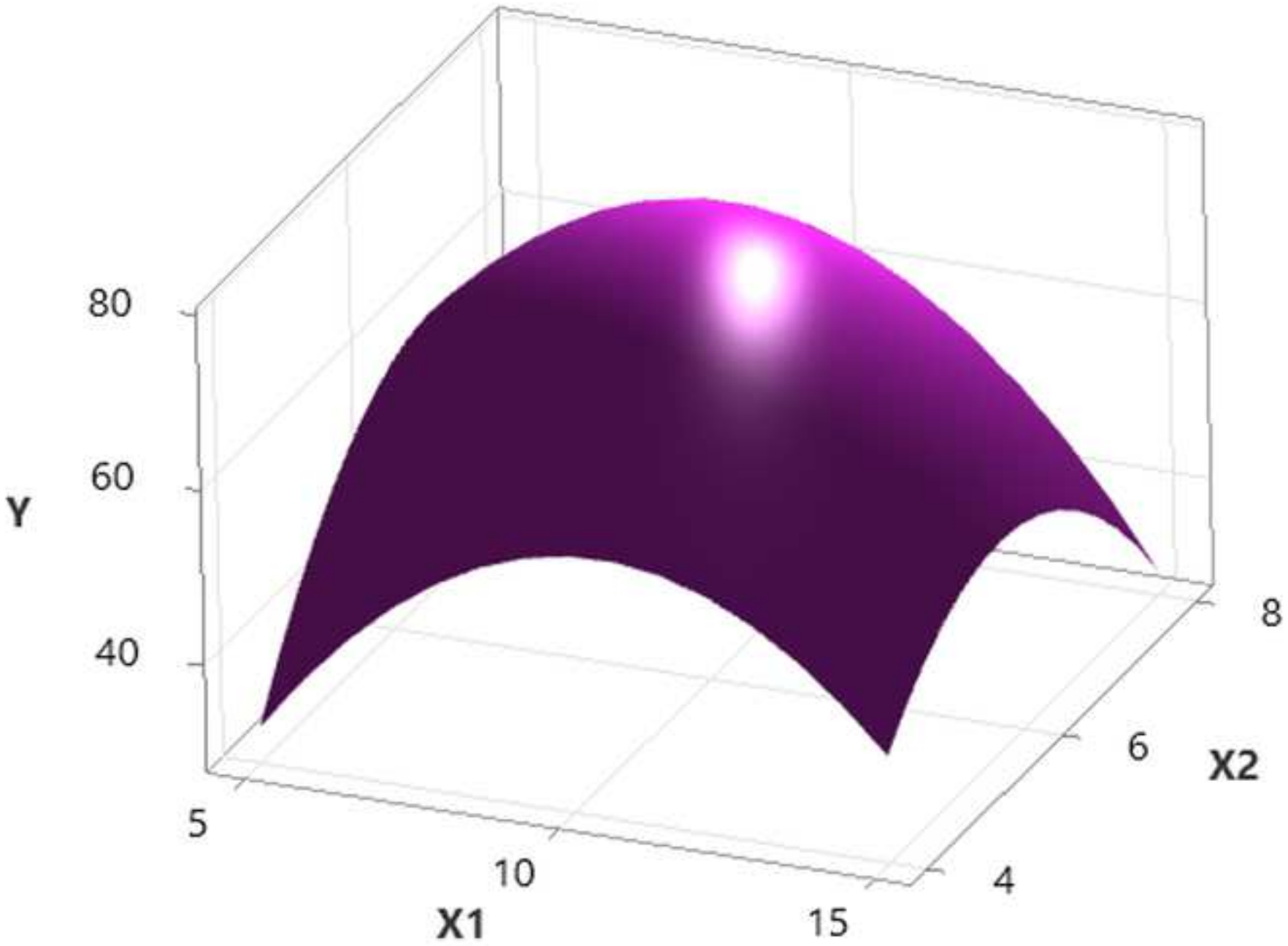

Figure

Click here to access/download;Figure;Figure_S13b.tif

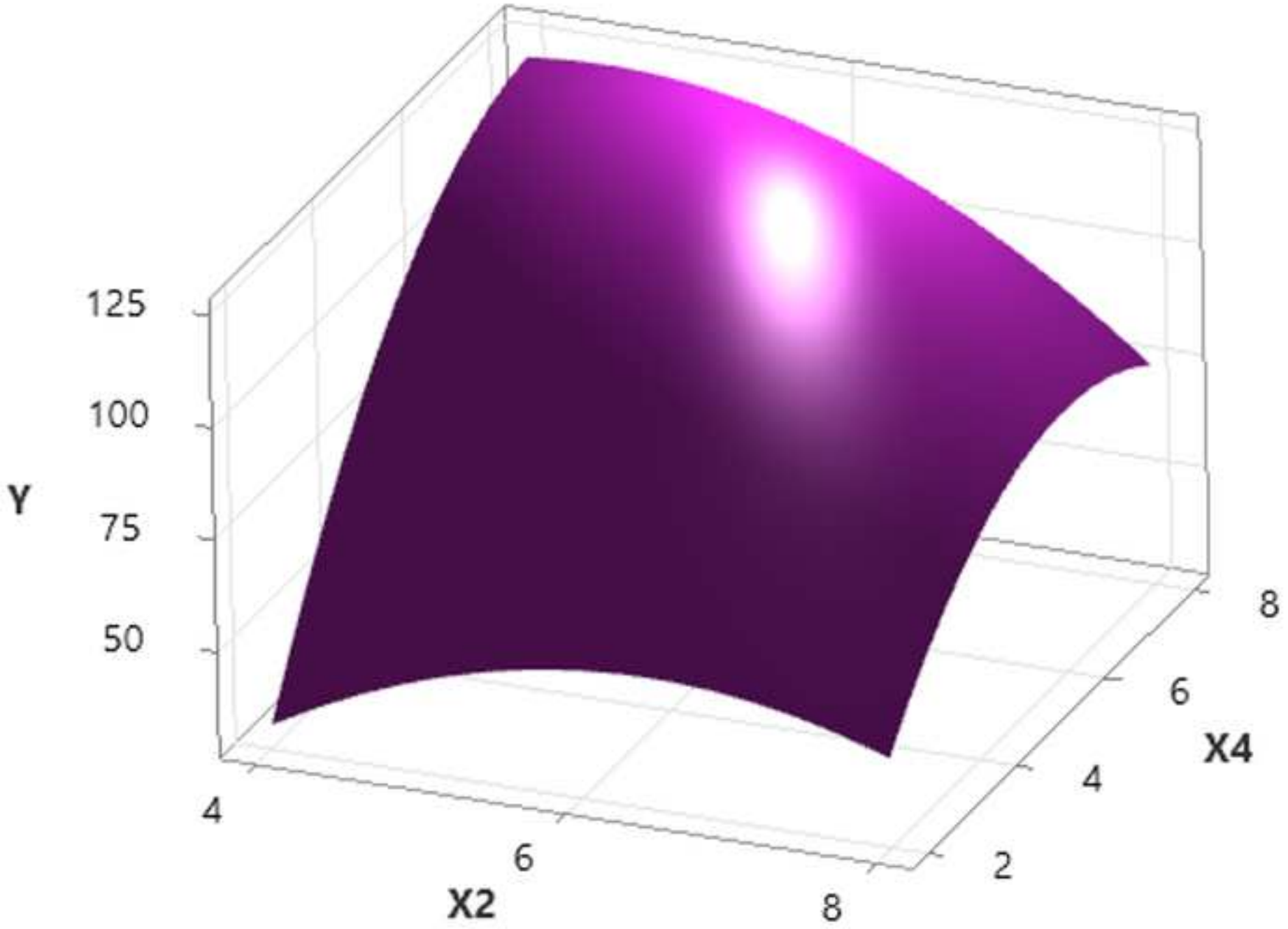

Caption of figures

Fig. 1. Comparison of the experimental PXRD patterns of NH_2-UiO-66, ChCl@NH_2-UiO-66.

Fig. 2. The FTIR spectra of NH_2-UiO-66 and ChCl@NH_2-UiO-66.

Fig. 3. SEM images of NH_2-UiO-66 (a-c), and ChCl@NH_2-UiO-66 (d-f).

Fig. 4. Energy dispersive X-ray spectroscopy (EDX) element mapping images of NH_2-UiO-66, and ChCl@NH_2-UiO-66.

Fig. 5. Thermogravimetric analysis of NH_2-UiO-66, and ChCl@NH_2-UiO-66.

Fig. 6. Specific Surface Area (BET) Analysis of Pristine NH_2-UiO-66, and Choline Chloride Functionalized NH_2-UiO-66 (ChCl@NH_2-UiO-66).

Fig. 7. Comparison of RE by ChCl@NH_2-UiO-66 and NH_2-UiO-66 under optimum conditions according to table 1.

Fig. 8. The impact of reusability cycles on RE of inhibitory compounds.

Fig. S1. A sample chromatogram obtained for a standard mixture of phenolic compounds at a concentration of 9.0 mg L^{-1} of the compounds.

Fig. S2. A sample chromatogram obtained for a standard mixture of phenolic compounds at a concentration of 9.0 mg L^{-1} of the compounds after the removal process.

Fig. S3. Calibration curve of (a) HQ, (b) HMF, (c) FF and (d) VAN.

Fig. S4. FTIR spectrum of the synthesized ChCl@MOF.

Fig. S5. FTIR spectra of HQ, MOF + HQ, ChCl@MOF + HQ.

Fig. S6. FTIR spectra of HMF, MOF + HMF, ChCl@MOF + HMF.

Fig. S7. FTIR spectra of FF, MOF + FF, ChCl@MOF + FF.

Fig. S8. FTIR spectra of VAN, MOF + VAN, ChCl@MOF + VAN.

Fig. S9. Surface plot of the cumulative effect of a) X1. X2; b) X1. X4 on RE of HMF.

Fig. S10. Surface plot of the cumulative effect of a) X1. X2; b) X1. X4 on RE of FF.

Fig. S11. Surface plot of the cumulative effect of a) X1. X2; b) X2. X3; c) X2. X4 on RE of HQ.

Fig. S12. Surface plot of the cumulative effect of X2. X4 on RE of VAN.

Fig. S13. Surface plot of the cumulative effect of a) X1. X2; b) X2. X4 on universal RE.